

See discussions, stats, and author profiles for this publication at: <https://www.researchgate.net/publication/301292703>

# Defect engineering of two-dimensional transition metal dichalcogenides

Article in 2D Materials · April 2016

DOI: 10.1088/2053-1583/3/2/022002

---

CITATIONS  
535

READS  
6,051

---

8 authors, including:



Zhong Lin  
Pennsylvania State University

77 PUBLICATIONS 6,798 CITATIONS

[SEE PROFILE](#)



Bruno R. Carvalho  
Universidade Federal do Rio Grande do Norte

30 PUBLICATIONS 1,393 CITATIONS

[SEE PROFILE](#)



Ruitao Lv  
Tsinghua University

173 PUBLICATIONS 9,311 CITATIONS

[SEE PROFILE](#)



Rahul Rao  
Air Force Research Laboratory

106 PUBLICATIONS 2,943 CITATIONS

[SEE PROFILE](#)

Some of the authors of this publication are also working on these related projects:



Energy storage [View project](#)



Band Gap Engineering through Hydrostatic Pressure [View project](#)

## Defect engineering of two-dimensional transition metal dichalcogenides

This content has been downloaded from IOPscience. Please scroll down to see the full text.

2016 2D Mater. 3 022002

(<http://iopscience.iop.org/2053-1583/3/2/022002>)

View the [table of contents for this issue](#), or go to the [journal homepage](#) for more

Download details:

IP Address: 130.203.95.138

This content was downloaded on 13/04/2016 at 17:43

Please note that [terms and conditions apply](#).

# 2D Materials



OPEN ACCESS

**TOPICAL REVIEW**

## Defect engineering of two-dimensional transition metal dichalcogenides

## RECEIVED

20 October 2015

## REVISED

10 December 2015

## ACCEPTED FOR PUBLICATION

11 January 2016

## PUBLISHED

13 April 2016

Original content from this work may be used under the terms of the Creative Commons Attribution 3.0 licence.

Any further distribution of this work must maintain attribution to the author(s) and the title of the work, journal citation and DOI.



Zhong Lin<sup>1,2</sup>, Bruno R Carvalho<sup>1,2,3</sup>, Ethan Kahn<sup>2,4</sup>, Ruitao Lv<sup>5</sup>, Rahul Rao<sup>6,7</sup>, Humberto Terrones<sup>8</sup>, Marcos A Pimenta<sup>3</sup> and Mauricio Terrones<sup>1,2,4,9,10</sup>

<sup>1</sup> Department of Physics, The Pennsylvania State University, University Park, PA 16802, USA

<sup>2</sup> Center for 2-Dimensional and Layered Materials, The Pennsylvania State University, University Park, PA 16802, USA

<sup>3</sup> Departamento de Física, Universidade Federal de Minas Gerais, Belo Horizonte, Minas Gerais 30123-970, Brazil

<sup>4</sup> Department of Materials Science and Engineering, The Pennsylvania State University, University Park, PA 16802, USA

<sup>5</sup> Key Laboratory of Advanced Materials (MOE), School of Materials Science and Engineering, Tsinghua University, Beijing 100084, People's Republic of China

<sup>6</sup> Air Force Research Laboratory, Materials and Manufacturing Directorate, RXAS, Wright-Patterson AFB, Ohio 45433, USA

<sup>7</sup> UES Inc., Dayton OH 45432, USA

<sup>8</sup> Department of Physics, Applied Physics and Astronomy, Rensselaer Polytechnic Institute, 110 Eighth Street, Troy, NY 12180, USA

<sup>9</sup> Department of Chemistry, The Pennsylvania State University, University Park, PA 16802, USA

<sup>10</sup> Institute of Carbon Science and Technology, Shinshu University, 4-17-1 Wakasato, Nagano-city 380-8553, Japan

E-mail: [mut11@psu.edu](mailto:mut11@psu.edu)(Mauricio Terrones)

**Keywords:** two-dimensional material, transition metal dichalcogenides, molybdenum disulfide, defects, electronic properties

### Abstract

Two-dimensional transition metal dichalcogenides (TMDs), an emerging family of layered materials, have provided researchers a fertile ground for harvesting fundamental science and emergent applications. TMDs can contain a number of different structural defects in their crystal lattices which significantly alter their physico-chemical properties. Having structural defects can be either detrimental or beneficial, depending on the targeted application. Therefore, a comprehensive understanding of structural defects is required. Here we review different defects in semiconducting TMDs by summarizing: (i) the dimensionalities and atomic structures of defects; (ii) the pathways to generating structural defects during and after synthesis and, (iii) the effects of having defects on the physico-chemical properties and applications of TMDs. Thus far, significant progress has been made, although we are probably still witnessing the tip of the iceberg. A better understanding and control of defects is important in order to move forward the field of Defect Engineering in TMDs. Finally, we also provide our perspective on the challenges and opportunities in this emerging field.

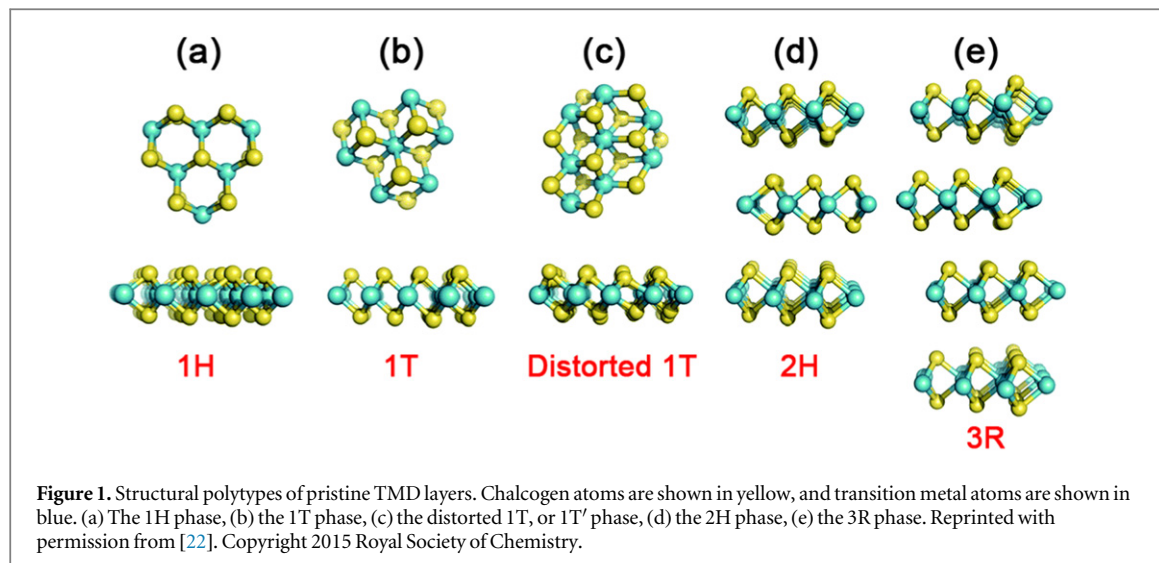
### 1. Introduction

As a result of thermal equilibrium and the kinetics of processing, all real materials contain structural defects which could significantly affect their properties. This statement is best represented by the development of the silicon semiconductor industry over 50 years. Engineering defects in silicon crystals constitutes a key approach to controlling the transport characteristics of silicon-based electronic devices. A critical example of this is the controlled implantation of charge donors and acceptors in silicon crystals to form p–n junctions.

Modern electronics require channel materials to be ultra-thin, and therefore two-dimensional (2D) materials are coming into play [1]. Graphene, a

prototype of all 2D materials, is not immune from structural defects [2–6]. Soon after the first exfoliation of graphene in 2004, several discrepancies between theory and experiment encouraged researchers to view graphene as a real material with defects [2–6], rather than an infinitely large 2D layer with perfect periodicity. Therefore, defect engineering has emerged as a key approach to understanding and modulating the properties of graphene.

It is now timely to start studying structural defects in other 2D materials, such as semiconducting transition metal dichalcogenides (sTMDs). Few-layered sTMDs, in a common form of  $MX_2$  ( $M = Mo, W$ ;  $X = S, Se$ ), exhibit numerous fascinating properties associated with their reduced thickness [7, 8]. For



example, sTMDs undergo a layer dependent transition in their band structure from an indirect to a direct band gap semiconductor [9, 10]. This transition immediately makes sTMDs attractive in electronics and optoelectronics [7, 11]. However, sTMD based devices show n- or p-type behavior, contradicting what one would expect from a perfect crystal structure without unsaturated bonds [12]. The typical device mobilities extracted from experiments also lie way below theoretical predictions [12]. Furthermore, photoluminescence (PL) measurements have resolved an emission peak within the optical band gap, which is again not consistent with the band structure derived based on a perfect crystal structure [13]. Raman spectroscopy has also revealed an intensity increase of the LA(M) mode, a phonon vibrational mode, as a function of crystalline disorder [14]. Such observations point to a simple fact: structural defects in sTMDs cannot simply be ignored [4, 15].

The motivation of this article is therefore to summarize (1) which kinds of structural defects have been observed in TMDs; (2) under what conditions structural defects are introduced into TMDs, and (3) to what extent structural defects alter the properties of TMDs. This article does not try to provide a comprehensive review about TMDs, which can be found elsewhere [7, 8, 16–21]. We wish to deliver the message to our readers that having structural defects in TMDs is not necessarily disappointing or puzzling. As the field progresses, it is expected to further understand defects in TMDs, and to explore the novel applications defects may enable.

The organization of this review is as follows: In section 2, we classify structural defects according their dimensionality and atomic structure. In section 3, we summarize typical experimental approaches to generate structural defects. In section 4, we discuss how structural defects significantly modulate electrical, optical, vibrational, magnetic, and chemical properties of the TMDs. In the last section, we provide our

perspective on future directions about defect engineering.

## 2. Classification of defects in TMDs

Before we discuss structural defects, we first introduce structure polytypes of the defect-free (or pristine) TMDs crystals (see figure 1) [22]. A single molecular layer of  $MX_2$  is formed by an atomic trilayer which consists of two adjacent layers of chalcogen atoms ( $X$ ) covalently bonded by a layer of transition metal atoms ( $M$ ) forming an  $X-M-X$  layer configuration. Two possible structural polytypes have been reported for a monolayer  $MX_2$ : the semiconducting trigonal prismatic phase (we adopt the notation 1H for monolayers; see figure 1(a); the 2H phase refers to bulk crystals), and the metallic octahedral prismatic phase (the 1T phase; see figure 1(b)) [23]. In certain cases, the 1T phase is not thermodynamically stable, and its structurally distorted derivative, denominated as 1T' can be observed instead (see figure 1(c)). When TMD crystals have more than one atomic chalcogen–metal–chalcogen ( $X-M-X$ ) layer of the 1H phase bonded by van der Waals (vdW) forces, additional polytypes appear in account for variations in stacking orders. A Bernal stacking (AbA BaB) yields the 2H phase (see figure 1(d)), while an AbA CaC BcB stacking yields a rhombohedral phase denominated as the 3R phase (see figure 1(e)).

All above structural polytypes have attracted considerable attention and have found themselves suitable for certain applications [22]. This review does not attempt to cover all those polytypes. We focus primarily on the semiconducting 1H and 2H phases.

After introducing pristine crystal structures, we now proceed to classify structural defects. By definition, 2D TMDs could be infinitely large within their basal planes, but are only atomically thin perpendicular to the planes. Consequently, defects residing in

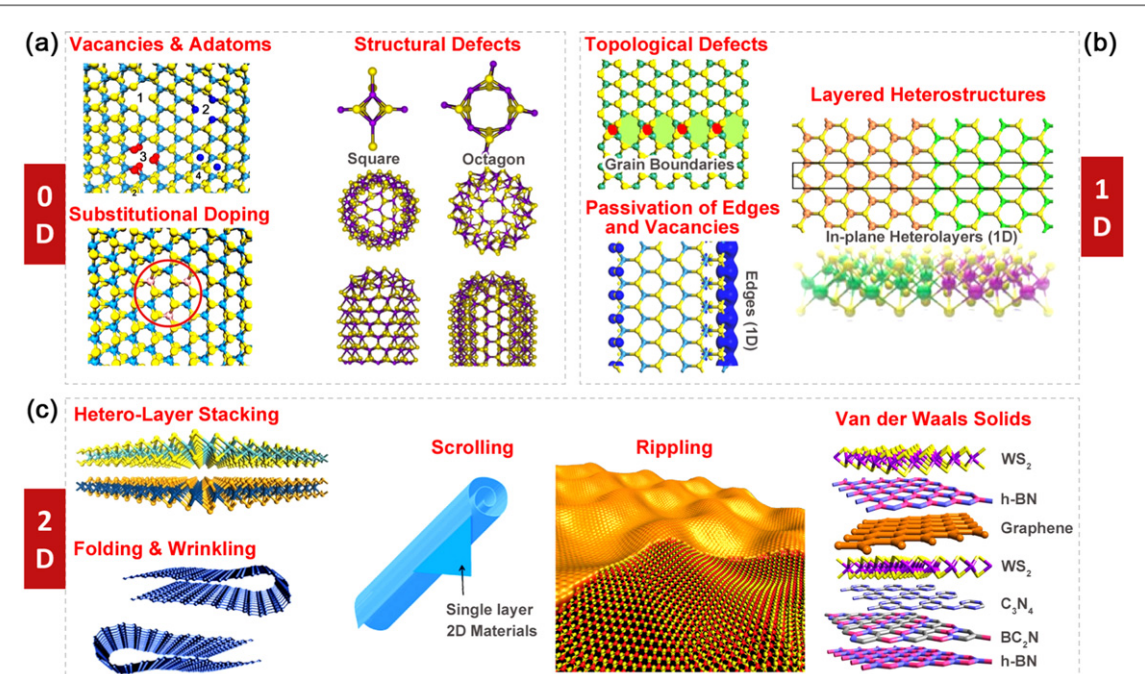


**Figure 2.** An overview of defects in 2D TMDs. (a) Typical zero-dimensional defects such as vacancies, adatoms, dopants, squares, and octagons. Reprinted with permission from [175]. Copyright 2000 American Physical Society. (b) Typical one-dimensional defects such as grain boundaries, edges, and phase interfaces. Reprinted with permission from [29]. Copyright 2014 Nature Publishing Group. (c) Typical two-dimensional defects such as folding, wrinkling, scrolling, rippling, and vertically stacked hetero-layers. Reprinted with permission from [111]. Copyright 2013 Nature Publishing Group. Reprinted with permission from [176]. Copyright 2012 American Chemical Society. Reprinted with permission from [177]. Copyright 2013 Wiley.

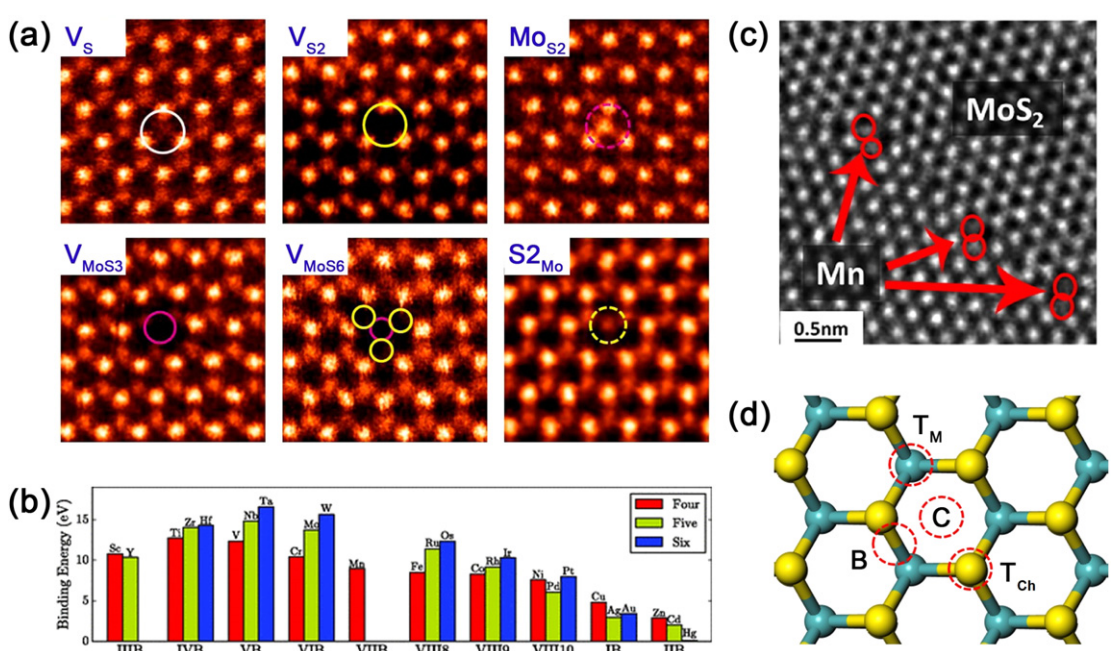


**Figure 3.** Zero-dimensional defects. (a) Atomic-resolution annular dark field (ADF) images showing different types of vacancy and vacancy complexes in MoS<sub>2</sub> monolayers. Reprinted with permission from [24]. Copyright 2013 American Chemical Society. (b) Comparison of binding energies for MoS<sub>2</sub> monolayers doped with transition metal atoms. Red, green and blue symbols correspond to dopants in group four, five and six, respectively. Reprinted with permission from [36]. Copyright 2013 American Physical Society. (c) TEM image showing MoS<sub>2</sub> monolayers substitutionally doped by Mn atoms. Reprinted with permission from [41]. Copyright 2015 American Chemical Society. (d) A schematic diagram showing four sites of adatoms adsorbed onto TMD lattices.

these 2D crystals could be classified according to their dimensionality as zero-dimensional (point defects, dopants or ‘non-hexagonal’ rings; see figure 2(a)), one-dimensional (grain boundaries, edges, and in-

plane heterojunctions; see figure 2(b)) and two-dimensional (layer stacking of different layers or vdW solids, wrinkling, folding, and scrolling; see figure 2(c)).

### 2.1. Zero-dimensional defects in TMDs

The simplest and most abundant defects in TMDs are vacancies, and the anti-sites that form on them (see figure 2(a)). In synthetic TMD samples, six varieties of intrinsic point defects are observed with regularity (see figure 3(a)): single sulfur vacancies ( $V_S$ ), double sulfur vacancies ( $V_{S2}$ ), a vacancy of a Mo atom and a triad of its bonded S within one plane ( $V_{MoS3}$ ), a vacancy of a Mo atom and all six of its nearest neighbors ( $V_{MoSe}$ ), an antisite, with Mo occupying a  $V_{S2}$  ( $Mo_{S2}$ ), and a pair of S atoms occupying a Mo position ( $S2_{Mo}$ ) [24]. The notable absence of  $V_{Mo}$  from this list is likely due to its tendency to complex with sulfur vacancies. With the exception of  $Mo_{S2}$ , reconstruction of the structure is minimal upon forming vacancies, and the defects retain trigonal symmetries [24, 25].  $V_S$  has the lowest formation energy of these defects ( $\sim 2$  eV) [24–27], but the exact value depends upon the chemical potentials  $\mu_{Mo}$  and  $\mu_S$ . Given thermal equilibrium,  $\mu_{MoS2} = \mu_{Mo} + 2\mu_S$  and both  $\mu_{Mo}$  and  $\mu_S$  must be less than their values in bulk (an ambiguous figure for S, given its many allotropes) [25], the chemical potentials are constrained to certain values. It is a boon to experimentalists when defect formation energy calculations consider the full range of values for  $\mu_{Mo}$  and  $\mu_S$  or at least the limiting sulfur rich and molybdenum rich conditions [25]. Without a full understanding of the thermodynamic parameters at play, it is a challenge to rationally produce defects on the lab bench.

It is also possible for other atomic species to replace lattice atoms by substituting elements. When considering the extent to which a foreign atom may substitute onto a crystal lattice, the ion's relative size, electronegativity, valence, and end member crystal structure are all relevant factors. The lanthanide contraction is a fortuitous periodic trend, which results in comparable radii for the 4d and 5d transition metals. This makes possible a wide variety of dopants from across the transition metal block. Notably, the similarity of W and Mo based on the criteria enumerated above allows for the formation of complete solid solutions in monolayer crystals [28]. In CVD grown TMD crystals, the extent of Mo/W alloying is heavily dependent on reaction kinetics, resulting in out- or in-plane heterostructures [29, 30], or a hybrid morphology [31]. S/Se alloying exhibits similar behavior [32–34]. While Mo/W and S/Se doping have been explored, there are few reports on the electronic and magnetic properties of other potential dopants (e.g. Mn, Co, Ni, etc.).

To date, almost the entirety of the transition metal series has been examined with density functional theory (DFT) as substitutional dopants in  $MoS_2$  [35–40]. As can be seen by the calculated binding energies of transition metal dopants (see figure 3(b)) [36], with the exception of  $d^9$  and  $d^{10}$  elements, the possibility of substituting transition metal atoms onto the lattice appears quite favorable. Several metallic dopants other

than W have already been observed experimentally in few to monolayer  $MoS_2$  films, including Mn (see figure 3(c)) [41], Nb [42, 43], Fe [44], Re [45], Au [45], and Co [46]. Similarly, substitution of many potential dopants onto chalcogen sites has been considered computationally [35, 39, 47]. While chalcogen site doping may be favorable in sulfur deficient crystals, excepting oxygen [48–51], to our knowledge no substitutive dopants have been identified experimentally. In addition to energy-dispersive x-ray spectroscopy (EDX) and x-ray photoelectron spectroscopy (XPS), two characterization techniques able to perform elemental and structural analysis of dopant atoms are the 'Z contrast' annular dark field microscopy (ADF) [52], a scanning transmission electron microscope (STEM) technique so called because of its sensitivity to differences in atomic number, and extended x-ray absorption fine structure, which can provide information such as coordination number and interatomic distances [43].

Rather than substituting onto the lattice, foreign atoms can be adsorbed to the crystal's surface. Such adatoms, are another form of defect that is of especial importance in 2D materials, due to their extreme aspect ratios. In the case of 1H phase TMDs, there are four positions available to an adsorbant (see figure 3(d)): above the metal atoms ( $T_M$ ), above the chalcogen atoms ( $T_{Ch}$ ), on a metal–chalcogen bond (B), and above or within the center of hexagonal voids (C) [53]. In multilayer flakes, the  $T_M$  and  $T_{Ch}$  sites are equivalent to intercalated species due to the 2H phase's stacking sequence [25]. In the case of electron donating alkali adatoms on  $MoS_2$ ,  $T_M$  sites are predicted to be most energetically stable with adsorption energies approaching  $-1$  eV in agreement with XPS data showing suppressed signal from the transition metal atoms [35, 54]. For many other potential adatoms [35, 53, 55], even more favorable adsorption energies have been predicted. Unsurprisingly, the most likely adatoms to be observed in  $MoS_2$  are Mo and S. While both adatom species have been observed on multiple sites via high angle ADF (HAADF) [24], it is predicted that S adatoms are stable only at  $T_S$ , while Mo may rest either at  $T_M$  or C [25]. Adatoms may be quite mobile under irradiation [45], and even at room temperature [35]. Thus, an understanding of adatom mobility may lead to insights into the kinetics and stability of TMD synthesis at elevated temperatures. Finally, we note that while not strictly zero-dimensional, some researchers have adsorbed molecular charge donors/acceptors to  $MoS_2$  flakes [56].

### 2.2. One-dimensional defects in TMDs

Extrinsic sulfur line vacancies result from the agglomeration of sulfur vacancies which are usually produced by electron bombardment [57]. Single- and double-line vacancies are observed experimentally, both aligned along the zig-zag direction (see figures 4(a) and

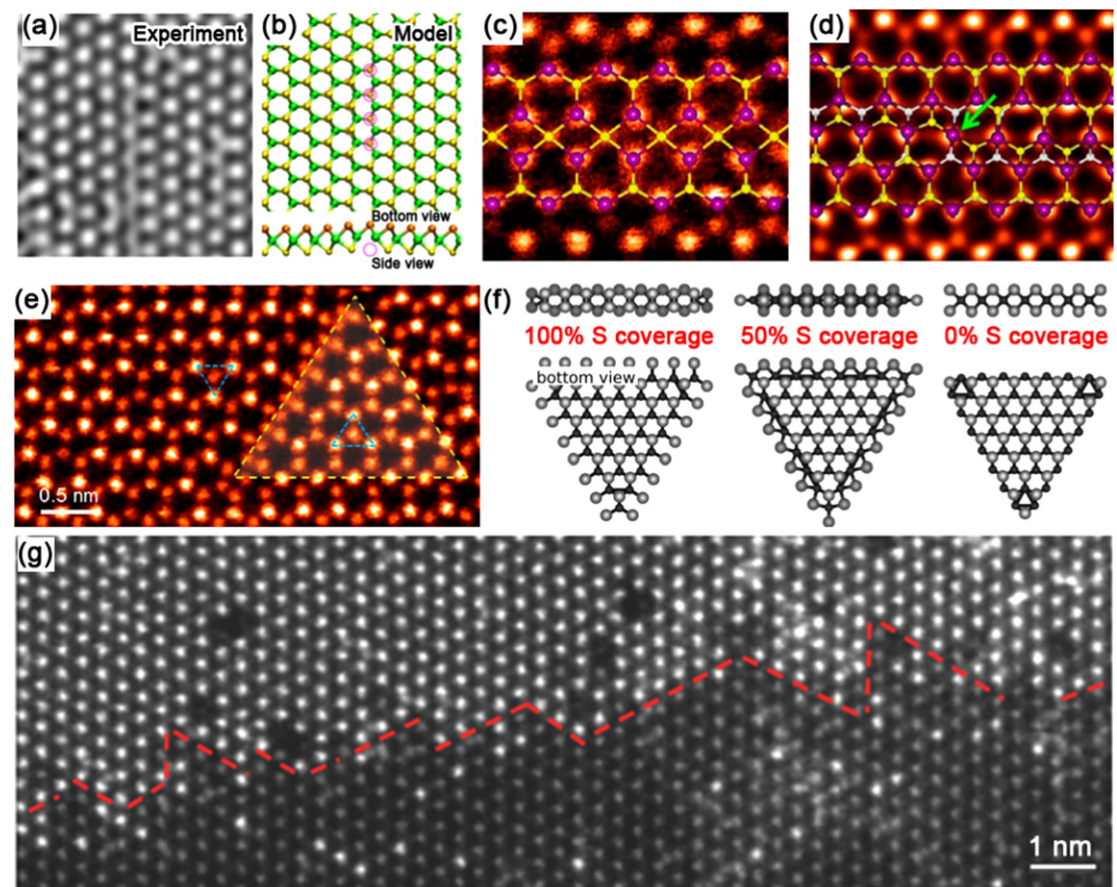


**Figure 4.** One-dimensional defects. (a) High-resolution transmission electron microscopy (HRTEM) image and (b) structural model showing a single vacancy line in  $\text{MoS}_2$  monolayers. Reprinted with permission from [57]. Copyright 2013 American Physical Society. (c) and (d) ADF images of 4l4P and 4l4E  $60^\circ$  grain boundaries in CVD  $\text{MoS}_2$  monolayers. Structural models are overlaid on ADF images. Reprinted with permission from [24]. Copyright 2013 American Chemical Society. (e) ADF image showing an inversion domain in monolayer  $\text{MoSe}_2$ . Reprinted with permission from [61]. Copyright 2015 American Chemical Society. (f) Structural models showing Mo-terminated  $\text{MoS}_2$  domains edges with different percentages of sulfur coverage. Reprinted with permission from [63]. Copyright 2002 Elsevier Science (USA). (g) ADF image showing a 1D interface between monolayer  $\text{MoS}_2$  and  $\text{WS}_2$ . Reprinted with permission from [29]. Copyright 2014 Nature Publishing Group.

(b)) [57]. This experimental result agrees with calculations which determine the formation energy of sulfur line vacancies in the zig-zag direction exhibit lower formation energies than those along the armchair direction [58]. In all cases, the formation energies of line vacancies are a function of the number of vacancies, in the range of 5–6 eV per vacancy for lengths of 6–16 [58]. When the freestanding edge regions are imaged by TEM, the orientation of line defects also depends on the strain. Thus, strain may serve as a means to select line vacancy orientations for tuning electronic properties [57].

In addition to sulfur line vacancies, grain boundaries are often observed in TMD monolayers. In comparison to one-atom-thick materials, TMD grain boundaries and the dislocation cores they are comprised of are quite complex. This is because three atomic layers compose TMD monolayers (i.e. chalcogen–metal–chalcogen). As atoms are removed, the structure relaxes in three dimensions, to form dreidel shaped dislocations with a variety of ringed motifs that are dependent on the grain boundary angle [59].

Patterns of two point-sharing four member rings (4l-4P) form mirror twin grain boundaries in synthetic  $\text{MoS}_2$  and  $\text{MoSe}_2$  [24, 60], when grains meet at  $60^\circ$  angles along the zig-zag direction (see figures 4(c) and (d)). 4l4E metallic edge-sharing line defects are another possible  $60^\circ$  grain boundary morphology, which can result in triangular inversion domains with metallic edges (see figure 4(e)) [61]. The situation becomes more complex for smaller angles, with 4l6, 4l8, 5l7, and 6l8 motifs appearing. HAADF-STEM shows that on these low angle, and high strain (up to 58%) grain boundaries, sulfur atoms are quite mobile, even under low accelerating voltages, resulting in dislocation movement [62].

We now turn our attention to the most prominent defects in TMD flakes, their edges. Synthetic TMD single-crystalline islands most often adopt triangular shapes with edges that appear sharp in microscopic images. The triangular morphology of these flakes can be explained through the 2D application of the Wulff construction, which simply states that low energy edges will be preferred. These surface energies are a

function of the  $\mu_S$ , or the sulfur vapor potential. When  $\mu_S$  is low (i.e., under low sulfur vapor pressures), MoS<sub>2</sub> will adopt distorted hexagonal shapes rather than triangles. Nanoscale calculations predict that under the sulfur rich conditions prevalent during TMD growth, (10̄10) Mo edges with either 50% or 100% S (see figure 4(f)) are the most thermodynamically stable [63]. Nevertheless, in CVD grown samples the Mo-terminated edges with both 0% and 50% S coverage have been observed, suggesting that CVD is a process away from equilibrium [24].

Lateral hetero-interfaces constitute another form of 1D defect. Lateral (inner/outer) heterostructures of MoS<sub>2</sub>/WS<sub>2</sub>, MoSe<sub>2</sub>/WSe<sub>2</sub>, MoS<sub>2</sub>/MoSe<sub>2</sub>, and WS<sub>2</sub>/WSe<sub>2</sub> have been reported recently [29, 30, 34]. Structurally coherent sharp interfaces (see figure 4(g)) have been observed as a result of covalent epitaxy between two dissimilar TMD layers with similar lattice constants.

### 2.3. Two-dimensional defects in TMDs

Perfect 2D materials have been predicted by theories as unstable upon thermal fluctuation, but after the discovery of graphene, it has gradually become clear that suspended graphene could stabilize by the formation of ripples, i.e., finite surface roughness and deformation [64]. Similarly, ripples with a typical height on the order of nm have been observed in as-synthesized MoS<sub>2</sub> monolayers (see figure 2(c)) [65, 66], and can be generated deliberately by scanning a laser beam over MoS<sub>2</sub> monolayers [67]. Ripples introduce strain into the materials, and could well affect their electronic properties [65, 68].

In few-layered TMDs, adjacent layers are coupled by vdW forces. The magnitude of vdW forces depends sensitively on the interlayer spacing, which is correlated to stacking configuration. Most synthetic few-layered TMDs exhibit a Bernal stacking (AbA BaB...), but derivations from this stacking configuration are also possible, especially when TMD layers are stacked manually via transfer techniques [69]. Due to the handling of TMDs, it is also possible for flakes to fold over onto themselves [70]. For those that assume the 1H phase, folding produces a structure distinct from the 2H phase. As we will discuss in section 4, the vdW interface has strong impact on the electronic and optical properties of few-layered TMDs, therefore the interface associated with a stacking and layer orientation can be viewed as a 2D defect (see figure 2(c)).

There is a large family of known 2D materials, such as graphene, hBN, TMDs, and layered oxides. Given the similarity in their interlayer ‘bonding’, 2D materials of different kinds can be placed one on top of another, forming vertical heterostructures or vdW solids (see figure 5(a)) [71]. When the top layer (e.g. MoS<sub>2</sub>) has a crystal structural similar to the bottom layer (e.g. graphene) (see figure 5(b)), their stacking occurs via vdW epitaxy [72]. Compared to covalent

epitaxy where adjacent layers are covalently bonded, vdW epitaxy is more tolerant to lattice mismatch between layers, thereby allowing a variety of 2D materials to be stacked in this way. The interfaces between vertical hetero-layers can also be viewed as 2D defects which generate new properties in the materials (see figure 2(c)). For example, when there is lattice mismatch, such as the cases of MoS<sub>2</sub>/MoSe<sub>2</sub> and WSe<sub>2</sub>/graphene, vdW epitaxy results in periodic Moiré patterns (see figure 5(c)) [73, 74], and each pattern results in different optoelectronic properties that need to be studied in more detail.

In closing our classification of defects, we draw attention to the possibility of TMD Haeckelites [75]. In defective graphene and carbon nanotubes, Haeckelites are extended areas of 5/7 ring defects [76, 77]. In analogy, the geometry of TMDs allows for the formation of 6/8 Haekelites (see figure 5(d)). The structure and electronic properties of TMD Haeckelites have been predicted for a wide number of TMD materials: the semiconducting TMDs of Mo and W become semi-metallic, while metallic NbS<sub>2</sub> and NbSe<sub>2</sub> become small gap semiconductors [75]. Therefore, achieving defect control in these 2D systems is very important in order to tailor their electronic, optical and even magnetic properties.

## 3. Generation of defects in TMDs

The following subsections describe possible ways to generate defects in 2D TMDs. For example, the introduction of structural defects such as atomic vacancies and grain boundaries could be achieved under fluctuating growth conditions using chemical vapor transport (CVT) or CVD. Those defects are often unintentionally generated. However, the structural defects can be more deliberately generated post-synthesis by several approaches, such as ion/electron irradiation, plasma treatments and high-temperature annealing in the presence of different gases. These methods have started to be studied but should continue to be developed in order to achieve defect type and concentration control in TMD materials.

### 3.1. *In situ* generation of defects in TMDs

Among all synthesis methods to grow stoichiometric and crystalline TMDs, CVT has been the most adopted one to grow bulk large TMD crystals. In general, CVT involves transport of vaporized TMD powders in a sealed ampoule with a temperature gradient along its length. Each CVT synthesis typically takes several days to assure high-quality crystal growth at temperatures around 1000 °C [78]. As-grown crystals usually exhibit high degree of crystallinity, are usually free of contamination from the transport agents (e.g. Br<sub>2</sub>, or I<sub>2</sub>), and have been used extensively for exfoliation and based proof-of-concept research. For example, field effect transistors (FETs) made from exfoliated TMD flakes

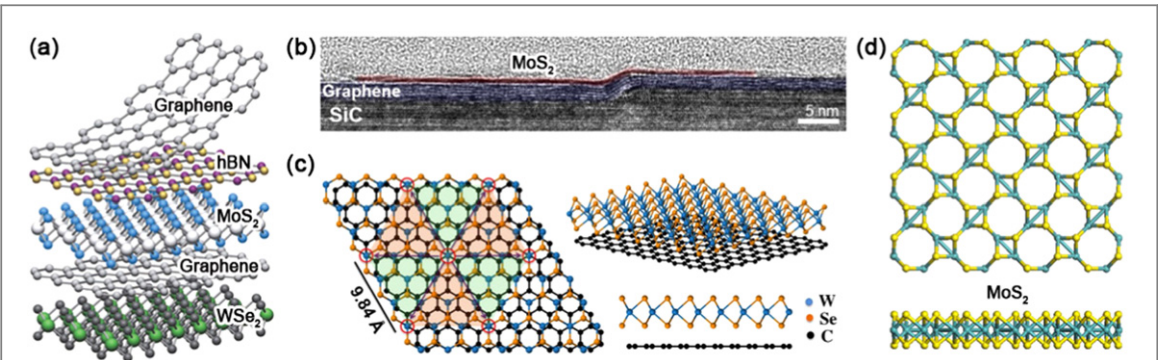


**Figure 5.** Two-dimensional defects. (a) Schematic representation of vdW heterostructures made by stacking different 2D materials. Reprinted with permission from [71]. Copyright 2013 Nature Publishing Group. (b) Cross-sectional transmission electron microscopy (TEM) image showing a 2D interface between MoS<sub>2</sub> and graphene layers. Reprinted with permission from [72]. Copyright 2014 American Chemical Society. (c) Structural model showing a Moiré pattern in vertically stacked monolayer WSe<sub>2</sub> and graphene. Reprinted with permission from [74]. Copyright 2015 American Chemical Society. (d) Relaxed structural models showing 8–4 MoS<sub>2</sub> Haeckelites. Reprinted with permission from [75]. Copyright 2014 Institute of Physics.

exhibit n-type (e.g. MoS<sub>2</sub>) or p-type (e.g. WSe<sub>2</sub>) behavior [11, 12], indicating that the channel materials are not defect-free. In fact, chalcogen vacancies and inversion domains have been observed in synthesized CVT crystals [79]. Each exfoliated flake naturally has edges, where the atomic structure and the chemical properties differ from the internal regions [80]. Besides single phase TMDs, CVT is also powerful in synthesizing doped (or alloyed) TMD bulk crystals [81]. Owing to the high growth temperature and long growth time, CVT grown crystals often possess structures with high spatial homogeneity. For example, CVT synthesized Mo<sub>x</sub>W<sub>1-x</sub>S<sub>2</sub> crystals show uniform distribution of Mo and W atoms in the entire crystal (see figure 6(e)) [28, 82], contrasting with CVD-synthesized Mo<sub>x</sub>W<sub>1-x</sub>S<sub>2</sub> alloys with an in-plane compositional gradient (see figures 6(b)–(d)) and CVD MoS<sub>2</sub>/WS<sub>2</sub> heterostructures with a well-defined phase boundary (see figure 6(a)) [29, 31]. Similarly, CVT MoS<sub>x</sub>Se<sub>2-x</sub> alloys have randomly distributed S and Se atoms, whereas CVD MoS<sub>x</sub>Se<sub>2-x</sub> monolayers can be homogeneous alloys [32, 33, 83], non-uniform alloys [84], or phase-segregated heterostructures [34]. If we consider substitutional dopants as point defects, CVT typically guarantees a uniform distribution of point defects (see figure 6(e)), and more importantly, the density of point defects could be fine-tuned by adjusting the initial loading of reactants. A variety of dopants have been added via CVT, for several purposes, such as band gap engineering (Mo<sub>x</sub>W<sub>1-x</sub>S<sub>y</sub>Se<sub>2-y</sub>) [28, 85, 86], and charge doping (p-type Nb doping [43], and n-type Re doping [45]), but additional work in this area is needed. Other metal and chalcogen dopants need now to be introduced in monolayers and bulk crystals of TMDs.

Besides top-down synthesis methods such as the aforementioned CVT-mechanical exfoliation, bottom-up approaches have also found wide applications

given their scalability. CVD is a typical bottom-up approach which involves chemical reduction of transition metal precursors by gaseous chalcogen precursors. When compared to CVT, CVD synthesis takes place on shorter time scales, at lower temperatures, and with more volatile precursors [87]. Owing to the relative violence of the technique, a large variety of defects can be generated and engineered in CVD-grown TMDs. For example, by adjusting the flow of sulfur vapor, it is possible to control the orientation and optical properties of domain edges, and the overall density of sulfur vacancies [88–90]. By varying the base pressure inside CVD reaction chambers, one can synthesize either isolated WS<sub>2</sub> triangular domains (see figure 6(f)) or quasi-continuous WS<sub>2</sub> films (see figure 6(g)) [88, 91, 92]. In principle, it is also possible to control the average grain size together with density of grain boundaries. By tuning growth temperatures during synthesis of MoS<sub>2</sub>/WS<sub>2</sub> heterostructures, one can selectively generate either 2D interfaces (see figures 6(h) and (i)) or 1D interfaces (see figures 6(j) and (k)) [29]. Different from CVT, a two-step growth is feasible via CVD. The second step provides additional degrees of freedom to modify the properties of the starting materials (materials obtained in the first step). Two-step growth is particularly powerful when the first and second step require sufficiently different growth conditions or precursors. Examples of two-step growths include partial sulfurization of CVD diselenides [93], partial selenization of CVD disulfides [93, 94], and formation of lateral junctions by *in situ* switching precursors [30, 34]. Another distinct feature of CVD is that the properties of resulting materials depend largely on the choice of substrates [95]. The flatness, lattice constants, thermal stability and cleanliness of substrates affect the density of grain boundaries, angle of grain boundaries, shape of domain edges, and domain orientations.

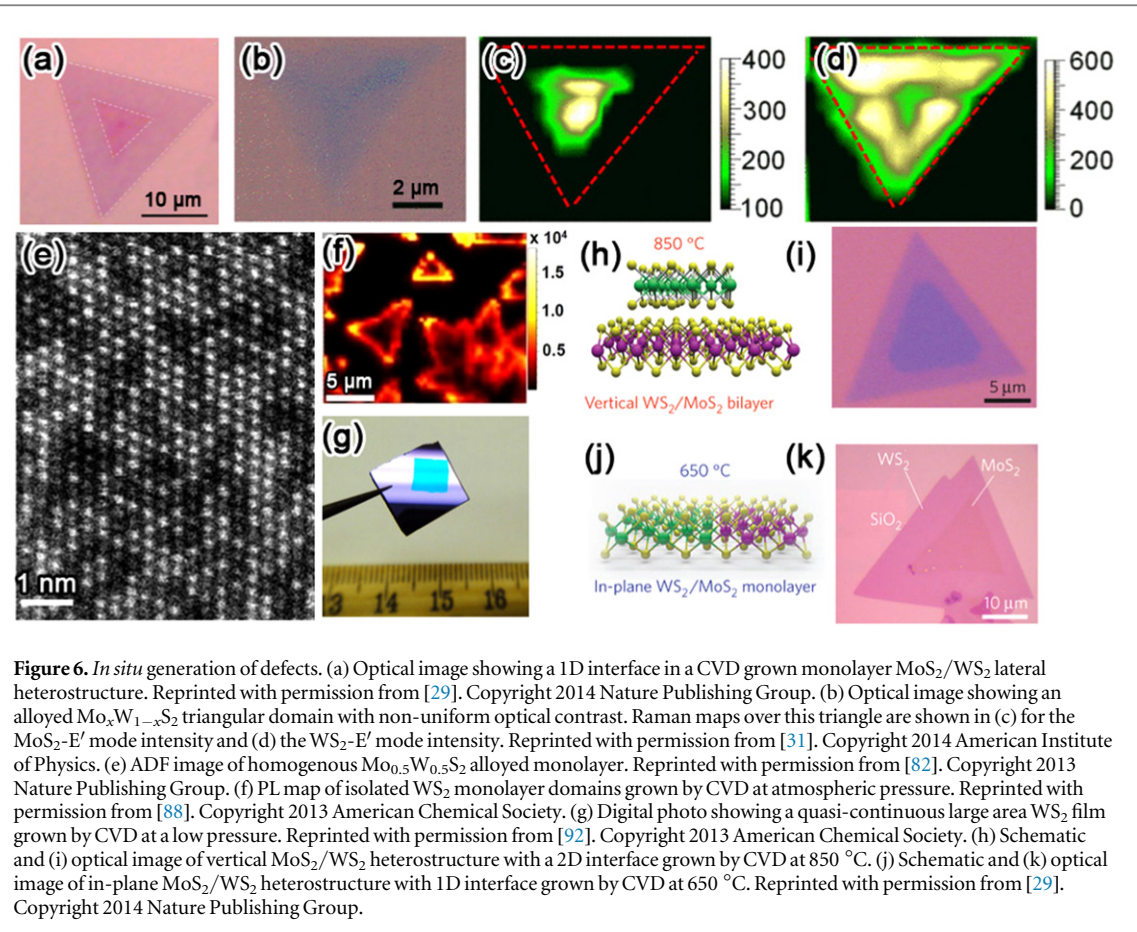


**Figure 6.** *In situ* generation of defects. (a) Optical image showing a 1D interface in a CVD grown monolayer MoS<sub>2</sub>/WS<sub>2</sub> lateral heterostructure. Reprinted with permission from [29]. Copyright 2014 Nature Publishing Group. (b) Optical image showing an alloyed Mo<sub>x</sub>W<sub>1-x</sub>S<sub>2</sub> triangular domain with non-uniform optical contrast. Raman maps over this triangle are shown in (c) for the MoS<sub>2</sub>-E' mode intensity and (d) the WS<sub>2</sub>-E' mode intensity. Reprinted with permission from [31]. Copyright 2014 American Institute of Physics. (e) ADF image of homogenous Mo<sub>0.5</sub>W<sub>0.5</sub>S<sub>2</sub> alloyed monolayer. Reprinted with permission from [82]. Copyright 2013 Nature Publishing Group. (f) PL map of isolated WS<sub>2</sub> monolayer domains grown by CVD at atmospheric pressure. Reprinted with permission from [88]. Copyright 2013 American Chemical Society. (g) Digital photo showing a quasi-continuous large area WS<sub>2</sub> film grown by CVD at a low pressure. Reprinted with permission from [92]. Copyright 2013 American Chemical Society. (h) Schematic and (i) optical image of vertical MoS<sub>2</sub>/WS<sub>2</sub> heterostructure with a 2D interface grown by CVD at 850 °C. (j) Schematic and (k) optical image of in-plane MoS<sub>2</sub>/WS<sub>2</sub> heterostructure with 1D interface grown by CVD at 650 °C. Reprinted with permission from [29]. Copyright 2014 Nature Publishing Group.

Bulk CVT- and CVD-synthesized disulfides and diselenides belong to the 2H phase (or 1H for monolayer). Chemically exfoliated disulfides sheets consist of 2H and 1T' phases [22]. The 1T' phase differs from the 2H phase in atomic structure and the electronic properties [22]. Here we would view the 1T' phase as an independent structural polytype rather than a defective derivative from the 2H phase (see figure 1). Therefore, the fascinating properties of the 1T' TMDs are unfortunately outside the scope of this article. Readers interested in this topic are encouraged to read a recent review by Voiry *et al* [22].

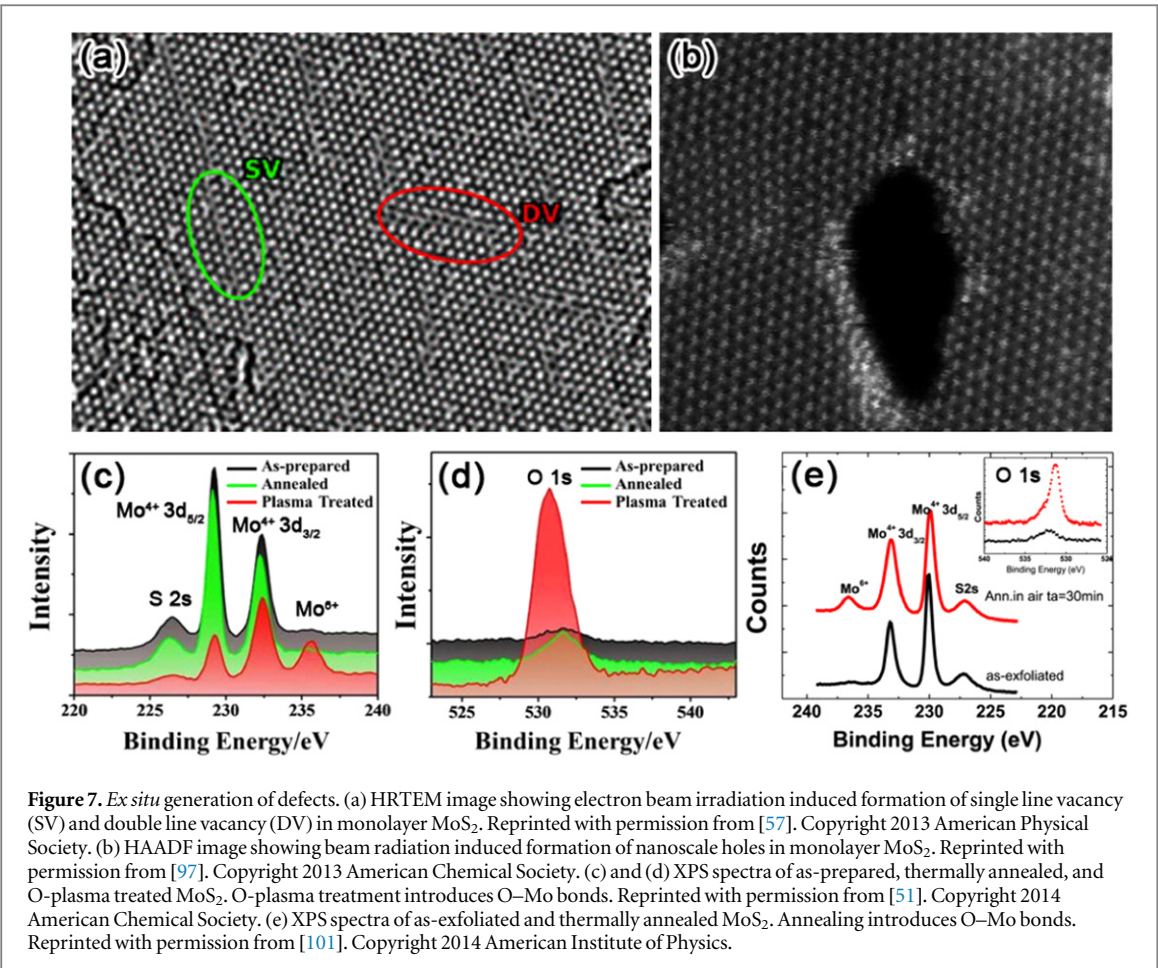
### 3.2. *Ex situ* generation of defects in TMDs

Besides *in situ* generation of defects during materials synthesis, recent progress also highlights the possibility of post-synthesis defect engineering. Previously, electron beam irradiation has been used to generate defects in graphene and hexagonal boron nitride (hBN) [5, 96]. Now this idea is extended to few-layered TMDs. First-principles calculations suggest that the threshold energy to generate chalcogen vacancies lies on the order of tens to hundreds of keV, which is accessible in state-of-the-art electron microscopes [47]. Indeed, sulfur vacancies are generated when TMD layers are subjected to energetic electron beams. The sulfur vacancies are mobile upon irradiation, migrating and agglomerating into vacancy lines (see figure 7(a)) or nanoscale holes if transition metal

atoms are also removed (see figure 7(b)) [57, 97]. Interestingly, the electron beam damage can be reduced by sandwiching TMD layers between graphene layers, possibly because the highly electric and thermal conductive graphene layers reduce the charge and heat accumulations [97].

Plasma treatment has also proven effective to generate a variety of defects in TMD layers. Oxygen plasma treatment introduces O–Mo bonds (see figures 7(c) and (d)) [49–51], while argon plasma can be used to create sulfur vacancies [98], and to even remove entire TMD layers [99]. Moreover, SF<sub>6</sub>, CF<sub>4</sub>, and CHF<sub>3</sub> plasma treatments can ripple and separate TMD layers [100]. In the future, it is possible that these techniques could be developed further in such a way that they could control the chemical functionalization and layer number in TMD or vdW systems. Further calculations on the effects of different functional groups or molecules on these systems should also be carried out.

Thermal annealing has also been employed to create sulfur vacancies and form Mo–O bonds in TMDs (see figure 7(e)) [13, 51, 101]. Alternative physical approaches for *ex situ* defects engineering include  $\alpha$  particle bombardment [13], Mn<sup>+</sup> ion bombardment [14], proton beam irradiation [102], ozone (O<sub>3</sub>) treatment [103], and laser illumination [80, 104], but detailed characterization studies on these defective systems are still needed.



#### 4. Properties and applications of defective TMDs

In the following subsections, we demonstrate how different defects can alter the properties of TMDs. In certain cases, defects can widen the potential applications of TMDs. In other cases, defects provide a limiting factor for reliability and homogeneity in otherwise pristine materials.

##### 4.1. Electronic properties of defective TMDs

As a semiconducting analogy to semi-metallic graphene and insulating hBN, MoS<sub>2</sub> has great potential in electronics and optoelectronics [11]. The device performance of atomically thin MoS<sub>2</sub> FETs depends on a variety of factors, including the material's quality, thickness, substrate, contacts, environment, and surface functionalization. Here we focus primarily on the effects of intrinsic structural defects on the transport characteristics. Zero-dimensional structural defects, such as sulfur vacancies (see figure 3(a)), are the most common defects in exfoliated and CVD MoS<sub>2</sub> monolayers [24]. Sulfur vacancies introduce unpaired electrons into the lattice, n-doping the material [105]. PL measurements and first-principles calculations reveal that sulfur vacancies lead to the formation of a non-zero density of states within the band gap [13, 24, 106].

Localized electronic states are created around sulfur vacancies, and when the carrier density is low, electrons transport via hopping between localized defect states [106]. In addition to sulfur-deficient MoS<sub>2</sub>, sulfur-rich (or molybdenum-deficient) MoS<sub>2</sub> has also been reported to show a p-type transfer behavior [105]. Both n- and p-type transports have been identified even from different regions of the same MoS<sub>2</sub> sample (see figures 8(a) and (b)). Thus, it is evident that further efforts should be devoted to the control of local stoichiometry. Other point defects such as foreign atoms can also alter the electronic properties of TMDs. Doped TMDs such as Mo<sub>x</sub>W<sub>1-x</sub>S<sub>2</sub>, Mo<sub>x</sub>W<sub>1-x</sub>Se<sub>2</sub> and MoS<sub>x</sub>Se<sub>2-x</sub> alloyed monolayers have been synthesized [28, 31–33, 82–86, 93, 94]. In these cases, doping induces an appreciable modulation in the band gap, as confirmed by PL measurements (see figure 8(c)). Notably, the band gap value does not change linearly with the stoichiometry, owing to the bowing effect [28]. Nb atoms can p-dope MoS<sub>2</sub>, which has been proposed theoretically and confirmed by transport measurements [35, 42, 43]. Re atoms are predicted by DFT to be n-type dopants [35], but experimental verification is lacking, and further measurements are needed.

1D defects such as vacancy lines, inversion domains, and grain boundaries also affect the

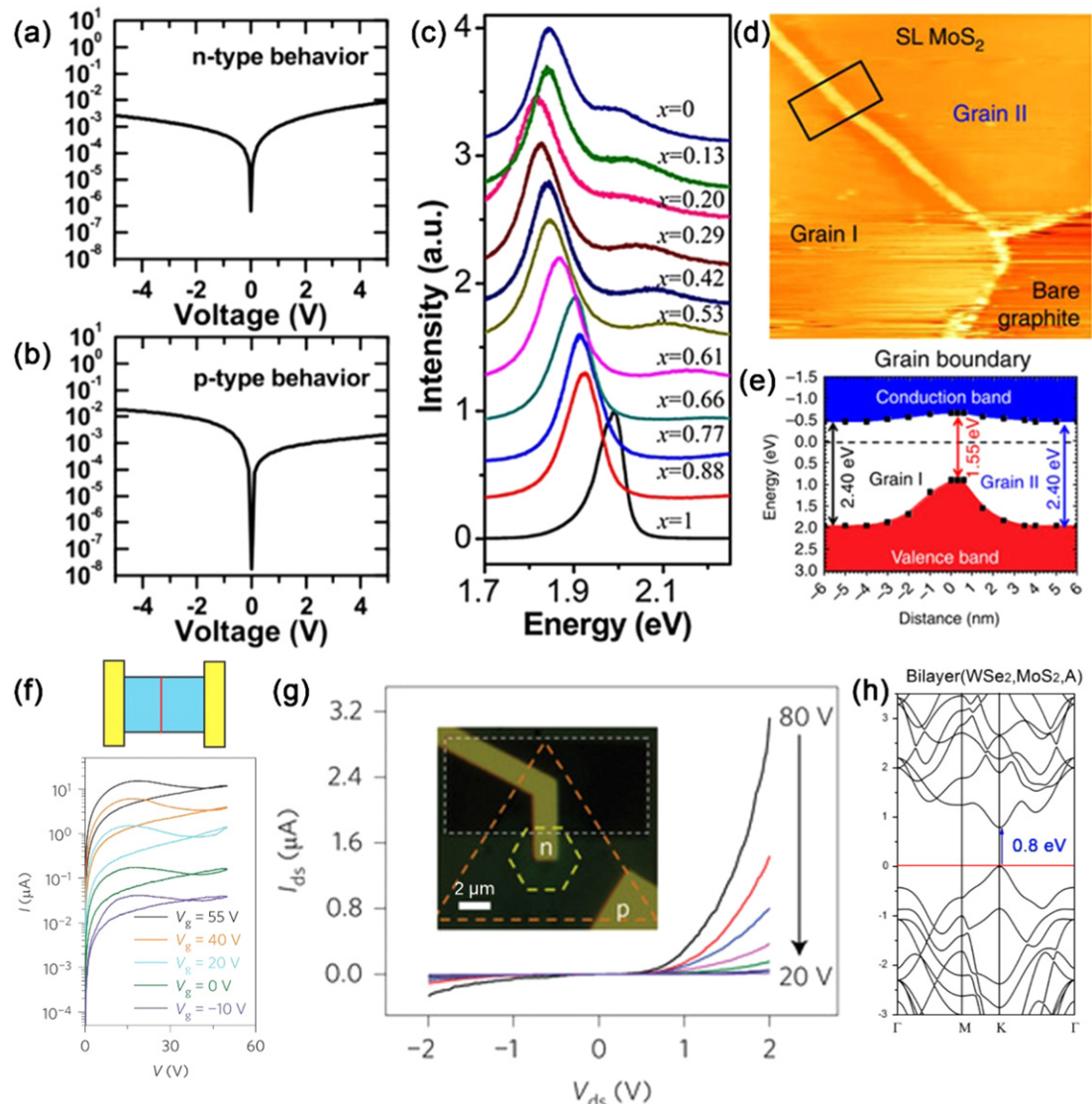


**Figure 8.** Electronic properties. (a) and (b)  $I$ – $V$  curves from MoS<sub>2</sub>/Au contacts. (a) and (b) are measured from different regions of the same sample, showing opposite transfer behaviors. Reprinted with permission from [105]. Copyright 2014 American Chemical Society. (c) PL spectra of alloyed Mo<sub>1-x</sub>W<sub>x</sub>S<sub>2</sub> monolayers with various compositions. Reprinted with permission from [28]. Copyright 2013 American Chemical Society. (d) STM image of monolayer MoS<sub>2</sub> with a grain boundary separating two grains. (e) Band gap profile in the proximity of the grain boundary shown in (d), measured by STS. Reprinted with permission from [107]. Copyright 2015 Nature Publishing Group. (f) Top: schematic representation of a memristor based on MoS<sub>2</sub> with a bisecting grain boundary. Bottom:  $I$ – $V$  curves showing gate-tunable memristive behaviors. Reprinted with permission from [110]. Copyright 2015 Nature Publishing Group. (g)  $I$ – $V$  characteristics showing a p–n diode behavior. The device is based on a lateral heterojunction composed of p-type WSe<sub>2</sub> and n-type WS<sub>2</sub> monolayers. An optical image of the device is shown as inset. Reprinted with permission from [34]. Copyright 2014 Nature Publishing Group. (h) DFT calculated band structure of WSe<sub>2</sub>/MoS<sub>2</sub> hetero-bilayers with the A-type stacking configuration. The direct gap transition is indicated by a vertical arrow. Reprinted with permission from [111]. Copyright 2013 Nature Publishing Group.

electronic properties of TMD layers. Sulfur line vacancies can interconnect into a triangular loop, encompassing an inversion domain rotated 60° from its surroundings. The change of stoichiometry at the edge of the inversion domains introduces mid-gap states, which are contributed primarily by the Mo orbitals [79]. Similarly, in MoSe<sub>2</sub> monolayers grown by molecular beam epitaxy, deviation from the stoichiometry in a Se-deficient condition leads to the formation of inversion domains defined by Se-deficit mirror twin boundaries. Theoretical calculations suggest that the conductance of the mirror twin boundaries is

enhanced as a result of additional spatially localized states within the band gap [60]. Depending on the atomic structures, grain boundaries in MoS<sub>2</sub> can be either sulfur-deficient or molybdenum-deficient, and therefore locally n-dope or p-dope the material [90]. Band gap variation in the proximity of grain boundaries have been detected by scanning tunneling microscope (STM)/ scanning tunneling spectroscopy (STS) (see figures 8(d) and (e)), suggesting local changes in the electronic structure [107]. Line defects can also reduce the rotational symmetry of the two-dimensional basal plane, and raise in-plane anisotropy in

quantum conductance [108]. Grain boundaries in CVD grown MoS<sub>2</sub> monolayers modulate the in-plane electrical conductivity [90], while grain boundaries in metal organic chemical vapor deposition (MOCVD) grown polycrystalline MoS<sub>2</sub> monolayer films show less disturbance on the spatial homogeneity of transport characteristics [109]. Although considerable efforts have been devoted to eliminating grain boundaries and building devices on large single crystalline MoS<sub>2</sub> domains, polycrystalline MoS<sub>2</sub> has recently found new applications in gate-tunable memristors where grain boundaries play an essential role (see figure 8(f)) [110]. Hetero-interfaces between two stitched dissimilar TMD monolayers are another type of 1D defect that have begun to draw attention. Recent advances in synthesis allow lateral epitaxial growth of MoS<sub>2</sub>/WS<sub>2</sub> and WS<sub>2</sub>/WSe<sub>2</sub> in-plane heterostructures, where the 1D interfaces serve as p-n junctions (see figure 8(g)) [29, 34].

When TMD monolayers are stacked along the vertical direction, the top layer interacts with the bottom layer via vdW force. The vdW interface can be viewed as a 2D defect which brings in new properties. For example, single phased semiconducting TMDs such as MoS<sub>2</sub> and WSe<sub>2</sub> experience a direct to indirect gap transition when the layer number goes beyond just one. However, first-principles calculations predict that hetero-bilayers are not necessarily indirect band gap semiconductors [111]. It is possible that a stacked hetero-bilayer has a direct band gap in energy lower than that of each constituent layer (see figure 8(h)) [111]. The electronic properties of homo- and hetero-bilayers depend on the original properties of each constituent layer, on the stacking angle and inter-layer spacing [29, 73, 112–121]. Moreover, new functionalities such as vertical rectifying junctions, photodiodes, and resonant tunneling diodes have been achieved in stacked MoS<sub>2</sub>/WSe<sub>2</sub> layers [122–124].

#### 4.2. Optical properties of defective TMDs

Optical properties of semiconducting TMD layers are strongly correlated to their electronic properties [7]. Defect induced changes in electronic band structure are often accompanied by appreciable changes in excitonic transitions [125]. An example given in section 4.1 shows that dopants induce band gap variation in semiconducting TMD monolayers, as well as a shift in the PL peak energy (see figure 8(c)). Beside the changes at band edges, subtle changes within the band gap can also introduce evident features in PL spectra. In exfoliated MoS<sub>2</sub> monolayers with bi-sulfur vacancies generated by controlled plasma irradiation, a PL peak is observed with an energy below the band gap value (see figure 9(a)), attributable to neutral excitons bound to defects [13, 125]. Edges, common 1D defects in CVD grown TMD triangular single-crystalline domains, emit visible light with intensity similar or higher than that from the interior regions

[88, 89]. The extraordinary edge PL emission can be understood by first principles calculations: with edge periodicity, transition metal valence states, and oxygen adsorption at edges taken into account, calculations show the edges of 2D TMDs can be semiconducting [126].

As discussed above, TMD layers are free of dangling bonds, and can be stacked vertically via vdW epitaxy. An atomically sharp 2D interface between adjacent layers can introduce novel optical properties that are absent in each layer when the stacked layers are sufficiently coupled. For example, as we have discussed in section 4.1, vdW stacking offers a possibility to tune the electronic band structure, and to enable new excitonic transitions in hetero-bilayers. This has been observed experimentally in mechanically stacked MoS<sub>2</sub>/WSe<sub>2</sub> bilayers, that showed a strong PL emission at ~1.50–1.56 eV, lower than the band gap energy of MoS<sub>2</sub> (~1.87 eV) and WSe<sub>2</sub> (~1.64 eV) (see figure 9(b)) [114]. Similarly, in CVD grown MoS<sub>2</sub>/WS<sub>2</sub> hetero-bilayers, a PL peak at lower energy (~1.4 eV) was observed [29]. Notably, this novel excitonic transition is spatially indirect, i.e. electrons and holes are from opposite layers due to type II band alignment in hetero-bilayers [114, 127].

TMDs could also share the same crystal structure and similar lattice constants, so they can be stitched together laterally without significant lattice misfit. MoS<sub>2</sub>/WS<sub>2</sub> and MoSe<sub>2</sub>/WSe<sub>2</sub> in-plane heterojunctions have been synthesized directly by vapor deposition methods [29, 30]. The transition from the first to the second phase occurs within an atomically sharp phase boundaries. The interface emits visible light with an energy lying between band gap values of the two phases, and with an intensity much stronger than those from both sides (see figure 9(c)) [29, 30].

Monolayer TMDs do not exhibit inversion symmetry, therefore certain nonlinear optical processes, such as second harmonic generation (SHG) are pronounced in monolayers [128–130]. The intensity of SHG signal depends on factors such as crystal orientation, excitation wavelength, and topological defects such as grain boundaries, and domain edges. In CVD grown polycrystalline MoS<sub>2</sub> monolayer films, SHG is reduced in intensity along grain boundaries as a result of destructive interference of waves from neighboring grains [131]. These grain boundaries, though atomically thin and optically invisible, can be directly mapped out by second harmonic microscopy (see figure 9(d)). Molybdenum terminated zig-zag domain edges, on the contrary, enhance second harmonic response locally, as a result of changes in the electronic properties at 1D edges, where the translational symmetry of the 2D domains is broken [131]. Ideally, 2H (or Bernal) stacked TMDs with an even number of layers do not generate second harmonic signal [128–130]. However, if even-layered TMDs have a non-ideal stacking configuration, the SHG is not necessarily quenched. It has been shown using artificially stacked

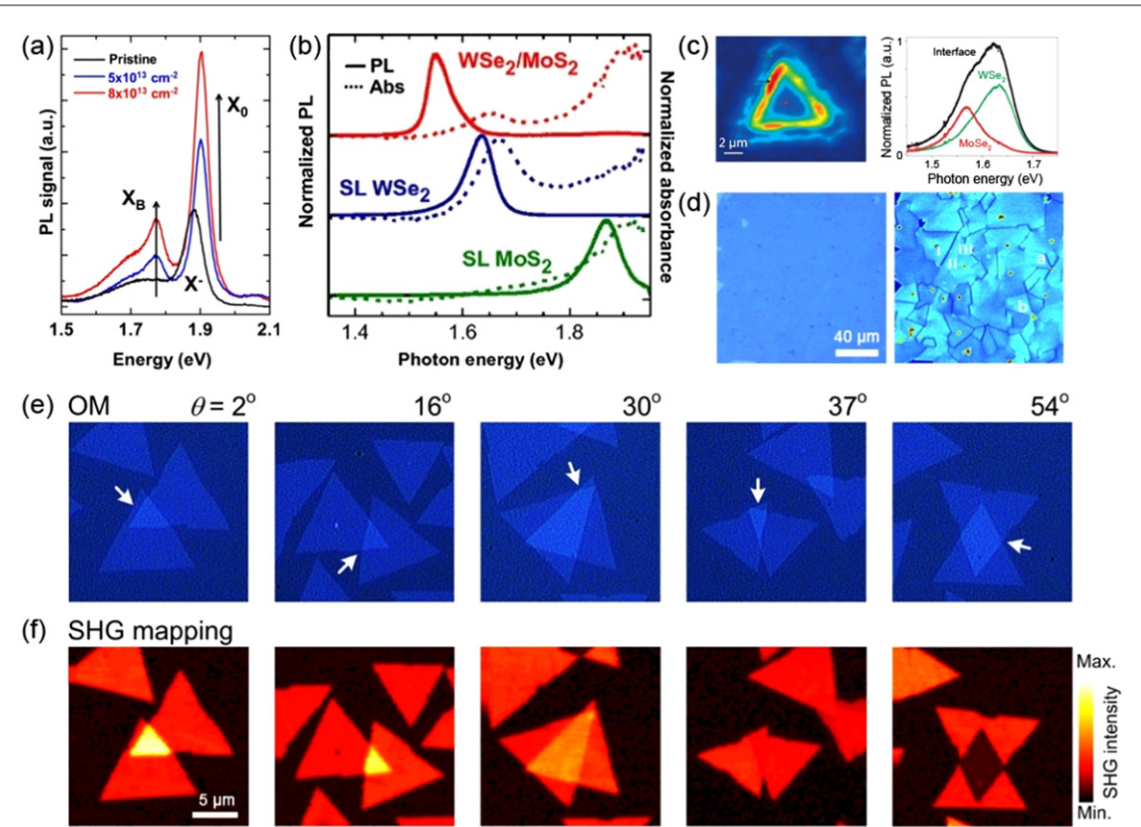


**Figure 9.** Optical properties. (a) Low temperature PL spectra at 77 K of pristine and  $\alpha$ -particle irradiated MoS<sub>2</sub> monolayers. Two irradiation doses used are  $5 \times 10^{13} \text{ cm}^{-2}$  and  $8 \times 10^{13} \text{ cm}^{-2}$ . Neutral, charged, and bound excitons are labeled as  $X^0$ ,  $X^-$ , and  $X^B$  respectively. Reprinted with permission from [13]. Copyright 2013 Nature Publishing Group. (b) Normalized PL and absorbance spectra for monolayer MoS<sub>2</sub>, WSe<sub>2</sub>, and their hetero-bilayers. Reprinted with permission from [114]. Copyright 2014 the National Academy of Sciences of the United States of America. (c) Left panel: PL intensity map of a MoSe<sub>2</sub>/WSe<sub>2</sub> lateral heterostructure. The colored arrows indicate regions of MoSe<sub>2</sub>, WSe<sub>2</sub> and their interface. PL spectra taken from indicated regions are shown on the right panel. Reprinted with permission from [30]. Copyright 2014 Nature Publishing Group. (d) Left panel: Optical image of a polycrystalline MoS<sub>2</sub> monolayer film. SHG image from the same area is shown in the right panel, where grain boundaries are visualized. Reprinted with permission from [131]. Copyright 2014 AAAS. (e) Optical images of artificially stacked MoS<sub>2</sub> bilayers with various stacking angle ( $\theta$ ). Their corresponding SHG intensity maps are shown in (f). Reprinted with permission from [69]. Copyright 2014 American Chemical Society.

MoS<sub>2</sub> bilayers that the SHG signal is recovered when the stacking order deviates from the intrinsic 2H stacking, owing to the lack of inversion symmetry [69]. Moreover, the intensity of SHG depends on the stacking angle which modulates the interference of second harmonic signal generated from each constituent TMD layer (see figures 9(e) and (f)). It is very likely that other nonlinear optical effects could be observed in different 2D systems, and research should concentrate on the synthesis of doped heterolayers.

#### 4.3. Vibrational properties of defective TMDs

Raman spectroscopy is an ideal and non-destructive technique to study the vibrational properties of 2D TMDs, as it provides rich information about different physical and structural properties of the samples [23, 78, 132–137]. In particular, Raman spectroscopy has been extensively used to identify number of layers [136, 138, 139], and to study the effects of charge-doping [140], strain [141, 142], and disorder [14, 96]. Interpreting Raman spectra of 2D TMDs requires understanding of the crystal symmetry. Here we

review briefly the symmetry of the 2D TMDs for the trigonal prismatic phases (i.e. 1H and 2H phases). The symmetries of TMDs are layer dependent. TMDs with an odd number of layers are non-centrosymmetric, whereas TMDs with an even number of layers are centrosymmetric [78]. The 1H phase has three Raman active phonon modes which are assigned to the irreducible representation of the D<sub>3h</sub> group as A'<sub>1</sub>, E' and E''. The A'<sub>1</sub> mode corresponds to the out-of-plane atomic displacement where the upper and lower layers of chalcogen atoms vibrate in-phase but in opposite directions. In the case of the E' and E'' modes, the atomic displacements are in the plane. The E' represents a mode in which the chalcogen atoms move in-phase and the metal atoms move in the opposite direction, whereas the E'' mode involves only the in-plane vibration of the chalcogen atoms, but in opposite directions. The E'' mode is forbidden in a common backscattering Raman experiment, in which the incident laser beam is perpendicular to the basal plane of TMD layers [136].

The bulk 2H TMDs have four first-order Raman active phonon modes represented by the irreducible representations of the  $D_{6h}$  group and are assigned as  $A_{1g}$ ,  $E_{1g}$ ,  $E'_{2g}$ , and  $E''_{2g}$ . The first three modes have similar origins as the  $A'_1$ ,  $E''$  and  $E'$  modes in the 1H polytype. Thus, the  $E_{1g}$  mode is also not observable in a common backscattering Raman experiment. The mode  $E''_{2g}$  originates from the vibration of adjacent rigid layers with respect to each other, and appears in the low-frequency range [136]. Note that above observable Raman modes originate from a first-order process and involve phonons only at the  $\Gamma$  point which is the center of the Brillouin zone (BZ) [136]. This constriction is a direct consequence of conservation of momentum. However, in the presence of structural defects which can serve as scattering centers to enable momentum conservation, phonon modes within the interior or at the edges of the BZ such as the longitudinal acoustic (LA) mode near and at the M and K points can be activated. Therefore by tracking the defect activated Raman modes, we can gather important information about structural defects [14, 96, 136, 143, 144].

Considering that many researchers in the 2D community are very familiar with Raman spectroscopy of graphene [143, 144], we first give an example of studying defective graphene by Raman scattering [96]. Figure 10(a) depicts a Raman spectrum of defective graphene, which displays three main Raman features, the D, G and 2D (or  $G'$ ) bands. Here D band play a key role in understanding defects. The G band corresponds to the  $E_{2g}$  phonon in the center of BZ. The D band is a disorder-induced band. This band involves an in-plane transverse optical (iTO) phonon near the K or  $K'$  points in the BZ that become Raman active activated via defects in the graphene lattice. For example, structural defects in graphene can be *ex situ* generated by ion irradiation. By changing the ion dose, one can change the average distance between defects ( $L_D$ ), or equivalently the defect density. As shown in the figure 10(b), the defect density has an evident correlation with the Raman intensity ratio of the D band over the G band, i.e.,  $I(D)/I(G)$ .

Similarly, defects in monolayer MoS<sub>2</sub> can be created intentionally via Mn<sup>+</sup> ion bombardment [14]. High dose of ion bombardment significantly enhances the relative intensity of the LA mode at M point (see figure 10(c)). The LA mode has a similar origin as the D-band in graphene since they both involve phonons near the edge of BZ and are activated by structural defects. Similar to defective graphene, in defective MoS<sub>2</sub> monolayers, the Raman intensity ratio  $I(LA)/I(A'_1)$  or  $I(LA)/I(E')$  could serve as an indicator to quantify the defect density (see figure 10(d)). Similarly, defects in other semiconducting chalcogenides such as WSe<sub>2</sub>, WS<sub>2</sub>, MoSe<sub>2</sub>, etc are also expected to be characterized by analyzing the evolution of the LA mode as well as other resonant modes such as 2LA at the M point as the number of defects increase within mono-

or few-layers. Progress along this direction is likely to be reported in due course.

The low-frequency range is relatively less explored for 2D materials, mainly due to the lower intensities of the low-frequency peaks compared to the E' and  $A'_1$  modes, and because these peaks typically lie outside the range ( $<100\text{ cm}^{-1}$ ) of conventional Raman spectroscopy systems. The two most significant peaks in the low frequency region for layered 2D materials are the rigid shear mode, involving the relative motion of atoms in adjacent layers, and the layer-breathing (LB) mode, involving out-of-plane displacements of atoms in adjacent layers. Naturally these modes are absent in the Raman spectrum from monolayer TMDs and only appear for two layers and above. The shear mode, also called the C mode for coupling, was first shown to vary in frequency as a function of graphene layers [145]. Similar to the case of graphene, the C mode has been measured by different groups in mono- and few-layered MoS<sub>2</sub> and WSe<sub>2</sub> [146–149]. For example, it is located at  $35\text{ cm}^{-1}$  for bulk MoS<sub>2</sub> and decreases in frequency down to  $\sim 20\text{ cm}^{-1}$  in bilayer MoS<sub>2</sub>. On the other hand, the LB mode, which is absent in bulk MoS<sub>2</sub>, increases in frequency. Since odd (even) layers lack (possess) inversion symmetry, the scaling of the C and LB modes are different with decreasing layer thickness [148, 149].

In addition to the C and LB modes, under resonant or near-resonant conditions (for example with a laser energy of 1.96 eV) a new peak has been observed at  $\sim 40\text{ cm}^{-1}$  in monolayer MoS<sub>2</sub> [147, 150]. Since this peak appears in the monolayer, it cannot be assigned to one of the rigid layer modes. Instead, the peak has been assigned to either electronic Raman scattering caused by the spin-orbit splitting of the conduction band [147], or to occurring from a strong resonance between excitons and polaritons [150]. Its origin is therefore unclear, and further theoretical and experimental works are required to fully understand the nature of this resonant peak.

Owing to the relative difficulty in obtaining spectral data in the low-frequency region, thus far low-frequency Raman spectroscopy has been the focus of just a few studies. With increasing opportunities for preparing heterostructures with different layered TMDs (vdW solids), the low-frequency modes are very useful for directly measuring interlayer coupling in 2D materials. Recent studies have shown the appearance of a new LB mode and suppression of the C mode in stacked MoS<sub>2</sub>/MoSe<sub>2</sub> and MoS<sub>2</sub>/WSe<sub>2</sub> heterostructures, whose frequency decreases with increasing stacking mismatch angle [151]. In addition, the relative intensities and frequencies of the C and LB modes have shown to vary (much more reliably than the high frequency modes) depending on stacking orientation (i.e. between the 2H and 3R configurations) in MoSe<sub>2</sub>/WSe<sub>2</sub> heterostructures [152]. Raman spectroscopy in the low frequency range therefore offers the opportunity to investigate the effect of dopants, interface

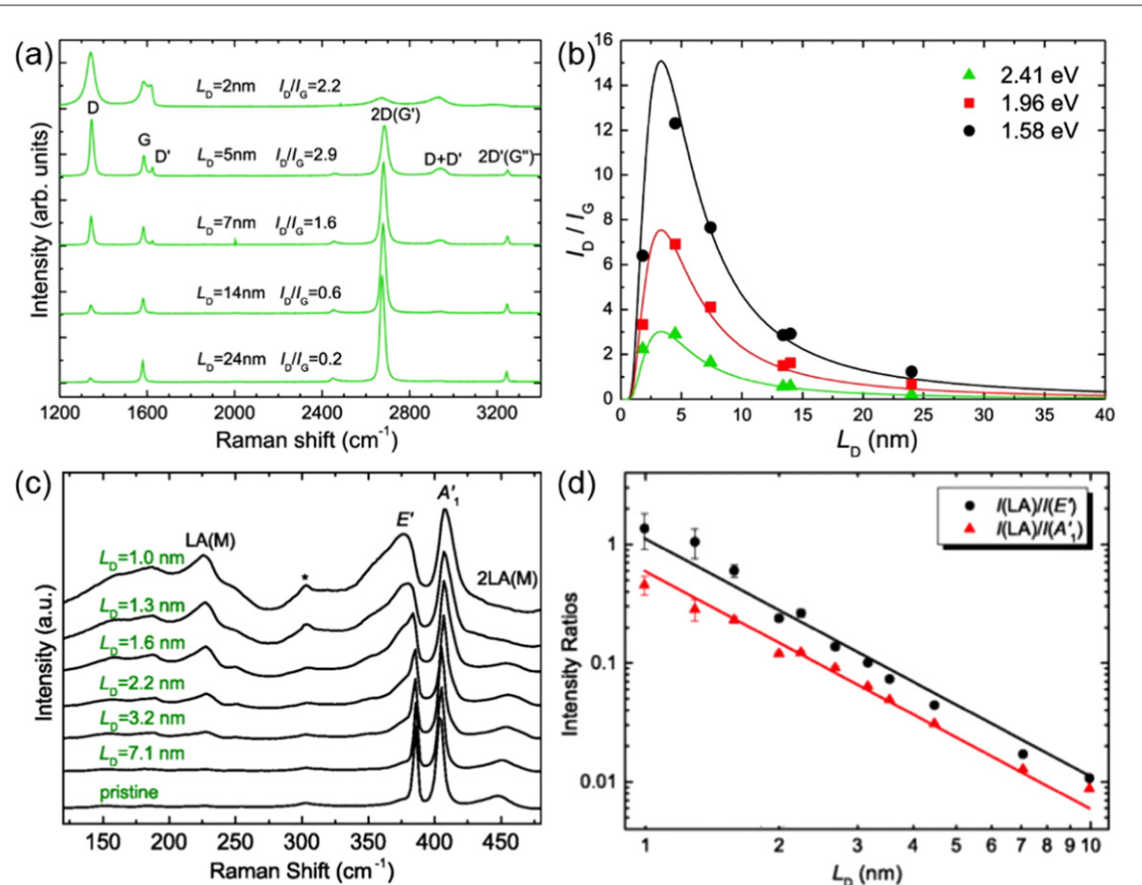


**Figure 10.** Vibrational properties. (a) Raman spectra of graphene with various defect densities, indicated by  $L_D$ . The laser energy used to measure is 2.41 eV. (b) Raman intensity ratio  $I(D)/I(G)$  of graphene with various defect densities. Laser energies used for measurements are 2.41, 1.96 and 1.58 eV. Reprinted with permission from [96]. Copyright 2011 American Chemical Society. (c) Raman spectra of monolayer MoS<sub>2</sub> with various defect densities, indicated by  $L_D$ . (d) Raman intensity ratio  $I(LA)/I(E')$  and  $I(LA)/I(A'_1)$  of monolayer MoS<sub>2</sub> with various defect densities. Laser energies used for measurements are 2.33 eV. Reprinted with permission from [14]. Copyright 2015 American Physical Society.

coupling, intercalants, and lattice mismatch in a wide variety of heterostructures or vdW solids composed of 2D TMDs.

#### 4.4. Magnetic properties of defective TMDs

Compared to the electronic and optical properties, the magnetic properties of layered MoS<sub>2</sub> and WS<sub>2</sub> remain less exploited. Diamagnetism and ferromagnetism have been observed in different samples of MoS<sub>2</sub> [153, 154], but the overall saturated magnetization in bulk MoS<sub>2</sub> is not large enough to be utilized in applications such as spintronics. To render MoS<sub>2</sub> truly magnetic, additional efforts have been made to tailor the material's microstructure. Irradiation has proven an effective method of enhancing ferromagnetism in bulk MoS<sub>2</sub>, presumably by generation of vacancies [153]. Scaling down the thickness of MoS<sub>2</sub> serves as another way to induce magnetism. Experimentally, several types of magnetism, including diamagnetism, paramagnetism and ferromagnetism have been identified in different samples of mono- and few-layered MoS<sub>2</sub> [155, 156]. Considering magnetic moments may be highly localized in samples, global magnetization measurements themselves may not provide enough

spatial resolution to discover the origins of magnetic ordering. To this end, first-principles calculations have shed some light. Spin polarized calculations suggest that one-dimensional edges of two-dimensional MoS<sub>2</sub> or WS<sub>2</sub> carry non-zero net magnetic moments associated with unpaired electrons (see figure 11(a)) [155, 157]. The edge ferromagnetism agrees with the experimental observation that TMD nanosheets possess larger magnetizations than their bulk counterparts. Grain boundaries also induce two types of long-range magnetic orderings in the host nanosheets depending on the tilt angles of grain boundaries [158]. Low angle boundaries composed of stitched 5/7 dislocation cores exhibit ferromagnetic behavior while high-angle boundaries' 4/8 rings are antiferromagnetic (see figure 11(b)). Besides utilizing native synthetic defects in TMDS, an alternative strategy to introduce magnetic ordering is to dope the materials. Therefore, the full series of 3d transition metal atoms, including Sc, Ti, V, Cr, Mn, Fe, Co, Ni, Cu and, Zn have been considered as substitutional dopants within the framework of DFT [36, 38, 40, 159–162]. Mn, in particular, seems to be a promising candidate for the introduction of long-range ferromagnetic ordering into the host

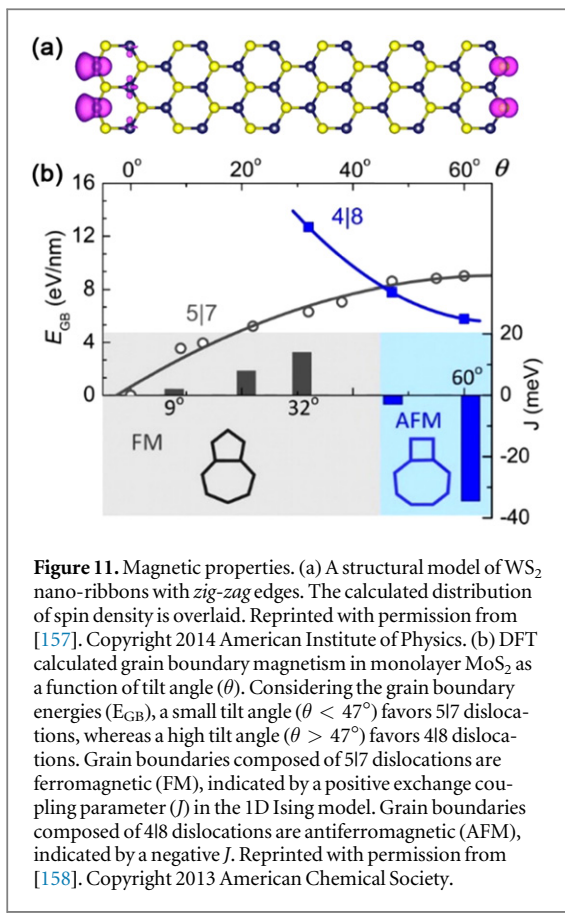


**Figure 11.** Magnetic properties. (a) A structural model of WS<sub>2</sub> nano-ribbons with zig-zag edges. The calculated distribution of spin density is overlaid. Reprinted with permission from [157]. Copyright 2014 American Institute of Physics. (b) DFT calculated grain boundary magnetism in monolayer MoS<sub>2</sub> as a function of tilt angle ( $\theta$ ). Considering the grain boundary energies ( $E_{GB}$ ), a small tilt angle ( $\theta < 47^\circ$ ) favors 5|7 dislocations, whereas a high tilt angle ( $\theta > 47^\circ$ ) favors 4|8 dislocations. Grain boundaries composed of 5|7 dislocations are ferromagnetic (FM), indicated by a positive exchange coupling parameter ( $J$ ) in the 1D Ising model. Grain boundaries composed of 4|8 dislocations are antiferromagnetic (AFM), indicated by a negative  $J$ . Reprinted with permission from [158]. Copyright 2013 American Chemical Society.

material [38, 40]. Significantly, calculations suggest Mn doped MoS<sub>2</sub> monolayers can exhibit a Curie temperature above room temperature, which is appealing for application in diluted magnetic semiconductors. Recently, doping Mn atoms into MoS<sub>2</sub> monolayers has been achieved by using a modified CVD process, in which dimanganese decacarbonyl (Mn<sub>2</sub>(CO)<sub>10</sub>) powders were added as Mn precursors, and graphene was used as a growth substrate [41]. Along this line, further experimental studies on Mn doping induced magnetism are expected.

#### 4.5. Chemical properties of defective TMDs

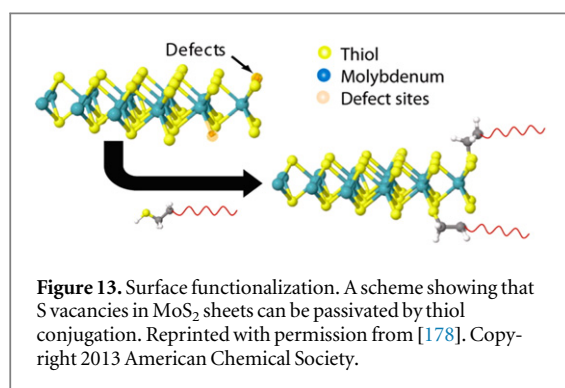
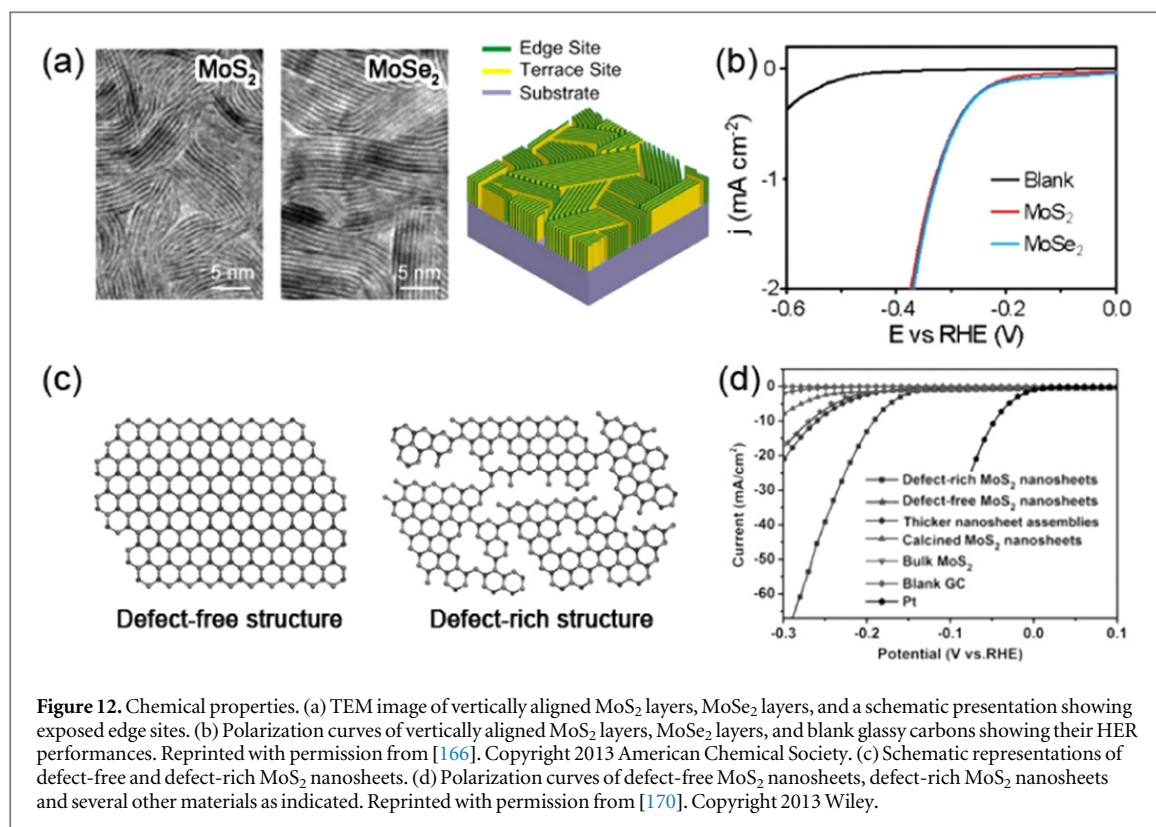
Because pristine TMD basal planes are largely chemically inert, introducing a reasonable amount of defects is crucial in chemical applications. MoS<sub>2</sub> can be extracted from mines and has long been considered as a low-cost catalyst for producing hydrogen, a clean alternative to fossil fuels, via hydrogen evolution reaction (HER) [163]. Bulk MoS<sub>2</sub> shows a relatively low catalytic activity, while when thinned down to few or monolayers the performance is significantly improved. Owing to the rapid progress in the synthesis of atomically thin layers, MoS<sub>2</sub> has been revisited in recent years as an effective catalyst [8, 20, 164]. The active sites for HER lie along one-dimensional edges of MoS<sub>2</sub> nanosheets while the basal planes are catalytically inert, as confirmed by recent experiments and DFT calculations [163, 165]. Efforts have been therefore made towards creating or exposing more active

edges. It has been demonstrated that by quickly sulfurizing molybdenum films deposited on a flat substrate, MoS<sub>2</sub> sheets are formed with basal planes perpendicular to the growth substrate, thereby exposing a high density of one-dimensional edges (see figures 12(a) and (b)) [166]. The vertically standing MoS<sub>2</sub> layers can also form on curved substrates such as nanotubes, in which case the density of exposed edges is further increased [167]. Another strategy to enhance catalytic performance is generating new edges via defect engineering [168]. The basal planes of MoS<sub>2</sub> sheets can be cracked chemically to introduce additional defects with unsaturated bonds (see figures 12(c) and (d)) [169, 170]. Besides increasing edge density, incorporating foreign atoms, introducing the metallic 1T phase, and forming nanocomposites, have also proven feasible strategies to make MoS<sub>2</sub> a more efficient catalyst [169, 171–174]. However, the possibilities are endless if we consider other TMDs different from MoS<sub>2</sub> and their heterostructures.

## 5. Conclusions and perspective

In this review, we have categorized structural defects in 2D semiconducting TMDs based on their dimensionalities and atomic structure. We have summarized pathways to generating structural defects, including *in situ* generation during the materials synthesis, and *ex situ* generation after synthesis. Defects significantly alter the original electrical, optical, vibrational, magnetic, and chemical properties of materials. However, it is encouraging that the effects of structural imperfections in 2D TMDs are not necessarily detrimental. In certain cases, defects provide benefits to material properties, enhancing device performance, and enabling unprecedented functionalities.

Given the short history of research on 2D TMDs, the study of their structural defects is still in its infancy and most of the work summarized here corresponds to MoS<sub>2</sub>. In the years to come, three complementary directions may become attractive to researchers entering this field. The first is to avoid defects by synthesizing high-quality materials. For example, efforts will continue towards increasing the grain size of CVD TMDs and reducing the number of grain boundaries. This direction is particularly important for proof-of-concept studies, for setting a baseline of the so-called intrinsic properties, and for applications which require large-scale spatial homogeneity such as electronics. The second potential direction is the rational creation and utilization of defects. Towards this end, more work about basal plane chemical functionalization (see figure 13) is expected as well as studies of how defects affect mechanical and thermal properties of TMDs. At present, atomic scale understanding and manipulation of defects remains a challenge. For example, the dynamics of local defect formation, migration and reconstruction are largely unexplored.



It is also challenging for experimentalists to introduce defects of specific types into desired locations and at controlled concentrations. The third potential direction is to heal defects, i.e. to convert defective TMDs into highly crystalline materials after synthesis. Given the high temperature and complicated dynamics during synthesis, it is impractical to fully avoid defects. Therefore, it may be necessary to develop approaches to eliminate certain synthetic defects after the fact. Recent advances in electron microscopy, optical spectroscopy, optoelectronics, and first-principles calculations have been bringing us new knowledge about defects on an almost daily basis. In light of this, it is not overly ambitious to expect breakthroughs in aforementioned directions to be on the horizon with joint efforts from physicists, chemists, materials scientists and engineers.

## Acknowledgments

This work was supported by the US Army Research Office MURI grant W911NF-11-1-0362, the Air Force Office of Scientific Research MURI grant FA9550-12-1-0471, by the Materials Simulation Center of the Materials Research Institute, the Research Computing and Cyberinfrastructure unit of Information Technology Services and Penn State Center for Nanoscale Science. MT acknowledges support from the Penn State Center for Nanoscale Science (DMR-0820404 and DMR-1420620). The authors acknowledge the Center for 2-Dimensional and Layered Materials at the Pennsylvania State University. BRC and MAP acknowledge the financial support of Brazilian agencies FAPEMIG, CNPq and CAPES, and the Brazilian Institute of Science and Technology (INCT) in Carbon Nanomaterials. RL acknowledges the support from the National Natural Science Foundation of China (Grant No. 51372131, 51232005) and 973 program of China (No. 2014CB932401, 2015CB932500). HT and MT acknowledge the financial support from the National Science Foundation (2DARE-EFRI-1433311 & 2DARE-EFRI-1542707). RR acknowledges funding from the Air Force Office of Scientific Research.

## References

- [1] Novoselov K, Jiang D, Schedin F, Booth T, Khotkevich V, Morozov S and Geim A 2005 Two-dimensional atomic crystals *Proc. Natl Acad. Sci. USA* **102** 10451

- [2] Hashimoto A, Suenaga K, Gloter A, Urita K and Iijima S 2004 Direct evidence for atomic defects in graphene layers *Nature* **430** 870
- [3] Terrones H, Lv R, Terrones M and Dresselhaus M S 2012 The role of defects and doping in 2D graphene sheets and 1D nanoribbons *Rep. Prog. Phys.* **75** 062501
- [4] Zou X and Yakobson B I 2015 An open canvas—2D materials with defects, disorder, and functionality *Acc. Chem. Res.* **48** 73
- [5] Banhart F, Kotakoski J and Krasheninnikov A V 2011 Structural defects in graphene *ACS Nano* **5** 26
- [6] Neto A C, Guinea F, Peres N, Novoselov K S and Geim A K 2009 The electronic properties of graphene *Rev. Mod. Phys.* **81** 109
- [7] Wang Q H, Kalantar-Zadeh K, Kis A, Coleman J N and Strano M S 2012 Electronics and optoelectronics of two-dimensional transition metal dichalcogenides *Nat. Nanotechnol.* **7** 699
- [8] Chhowalla M, Shin H S, Eda G, Li L J, Loh K P and Zhang H 2013 The chemistry of two-dimensional layered transition metal dichalcogenide nanosheets *Nat. Chem.* **5** 263
- [9] Mak K F, Lee C, Hone J, Shan J and Heinz T F 2010 Atomically thin MoS<sub>2</sub>: a new direct-gap semiconductor *Phys. Rev. Lett.* **105** 136805
- [10] Splendiani A, Sun L, Zhang Y, Li T, Kim J, Chim C Y, Galli G and Wang F 2010 Emerging photoluminescence in monolayer MoS<sub>2</sub> *Nano Lett.* **10** 1271
- [11] Jariwala D, Sangwan V K, Lauhon L J, Marks T J and Hersam M C 2014 Emerging device applications for semiconducting two-dimensional transition metal dichalcogenides *ACS Nano* **8** 1102
- [12] Schmidt H, Giustiniano F and Eda G 2015 Electronic transport properties of transition metal dichalcogenide field-effect devices: surface and interface effects *Chem. Soc. Rev.* **44** 7715
- [13] Tongay S et al 2013 Defects activated photoluminescence in two-dimensional semiconductors: interplay between bound, charged, and free excitons *Sci. Rep.* **3** 2657
- [14] Mignuzzi S, Pollard A J, Bonini N, Brennan B, Gilmore I S, Pimenta M A, Richards D and Roy D 2015 Effect of disorder on Raman scattering of single-layer MoS<sub>2</sub> *Phys. Rev. B* **91** 195411
- [15] Najmaei S, Yuan J, Zhang J, Ajayan P and Lou J 2015 Synthesis and defect investigation of two-dimensional molybdenum disulfide atomic layers *Acc. Chem. Res.* **48** 31
- [16] Butler S Z et al 2013 Progress, challenges, and opportunities in two-dimensional materials beyond graphene *ACS Nano* **7** 2898
- [17] Ganatra R and Zhang Q 2014 Few-layer MoS<sub>2</sub>: a promising layered semiconductor *ACS Nano* **8** 4074
- [18] Lv R, Robinson J A, Schaak R E, Sun D, Sun Y, Mallouk T E and Terrones M 2015 Transition metal dichalcogenides and beyond: synthesis, properties, and applications of single- and few-layer nanosheets *Acc. Chem. Res.* **48** 56
- [19] Wang H, Yuan H, Sae Hong S, Li Y and Cui Y 2015 Physical and chemical tuning of two-dimensional transition metal dichalcogenides *Chem. Soc. Rev.* **44** 2664
- [20] Huang X, Zeng Z and Zhang H 2013 Metal dichalcogenide nanosheets: preparation, properties and applications *Chem. Soc. Rev.* **42** 1934
- [21] Lv R, Terrones H, Elias A L, Perea-Lopez N, Gutierrez H R, Cruz Silva E, Rajukumar L P, Dresselhaus M S and Terrones M 2015 Two-dimensional transition metal dichalcogenides: clustes, ribbons, sheets and more *Nano Today* **10** 559
- [22] Voiry D, Mohite A and Chhowalla M 2015 Phase engineering of transition metal dichalcogenides *Chem. Soc. Rev.* **44** 2702
- [23] Wilson J and Yoffe A 1969 The transition metal dichalcogenides discussion and interpretation of the observed optical, electrical and structural properties *Adv. Phys.* **18** 193
- [24] Zhou W, Zou X, Najmaei S, Liu Z, Shi Y, Kong J, Lou J, Ajayan P M, Yakobson B I and Idrobo J C 2013 Intrinsic structural defects in monolayer molybdenum disulfide *Nano Lett.* **13** 2615
- [25] Komsa H-P and Krasheninnikov A V 2015 Native defects in bulk and monolayer MoS<sub>2</sub> from first principles *Phys. Rev. B* **91** 125304
- [26] Noh J-Y, Kim H and Kim Y-S 2014 Stability and electronic structures of native defects in single-layer MoS<sub>2</sub> *Phys. Rev. B* **89** 205417
- [27] Liu D, Guo Y, Fang L and Robertson J 2013 Sulfur vacancies in monolayer MoS<sub>2</sub> and its electrical contacts *Appl. Phys. Lett.* **103** 183113
- [28] Chen Y, Xi J, Dumcenco D O, Liu Z, Suenaga K, Wang D, Shuai Z, Huang Y S and Xie L 2013 Tunable band gap photoluminescence from atomically thin transition-metal dichalcogenide alloys *ACS Nano* **7** 4610
- [29] Gong Y et al 2014 Vertical and in-plane heterostructures from WS<sub>2</sub>/MoS<sub>2</sub> monolayers *Nat. Mater.* **13** 1135
- [30] Huang C, Wu S, Sanchez A M, Peters JJ, Beanland R, Ross J S, Rivera P, Yao W, Cobden D H and Xu X 2014 Lateral heterojunctions within monolayer MoSe<sub>2</sub>–WSe<sub>2</sub> semiconductors *Nat. Mater.* **13** 1096
- [31] Lin Z, Thee M T, Elias A L, Feng S M, Zhou C J, Fujisawa K, Perea-Lopez N, Carozo V, Terrones H and Terrones M 2014 Facile synthesis of MoS<sub>2</sub> and Mo<sub>x</sub>W<sub>1-x</sub>S<sub>2</sub> triangular monolayers *APL. Mater.* **2** 092514
- [32] Li H, Duan X, Wu X, Zhuang X, Zhou H, Zhang Q, Zhu X, Hu W, Ren P and Guo P 2014 Growth of alloy MoS<sub>2x</sub>Se<sub>2(1-x)</sub> nanosheets with fully tunable chemical compositions and optical properties *J. Am. Chem. Soc.* **136** 3756
- [33] Gong Y et al 2014 Band gap engineering and layer-by-layer mapping of selenium-doped molybdenum disulfide *Nano Lett.* **14** 442
- [34] Duan X et al 2014 Lateral epitaxial growth of two-dimensional layered semiconductor heterojunctions *Nat. Nanotechnol.* **9** 1024
- [35] Dolui K, Rungger I, Pemmaraju C D and Sanvito S 2013 Possible doping strategies for MoS<sub>2</sub> monolayers: an *ab initio* study *Phys. Rev. B* **88** 075420
- [36] Cheng Y, Zhu Z, Mi W, Guo Z and Schwingenschlögl U 2013 Prediction of two-dimensional diluted magnetic semiconductors: doped monolayer MoS<sub>2</sub> systems *Phys. Rev. B* **87** 100401
- [37] Feng N, Mi W, Cheng Y, Guo Z, Schwingenschlögl U and Bai H 2014 First principles prediction of the magnetic properties of Fe–X<sub>6</sub> (X = S, C, N, O, F) doped monolayer MoS<sub>2</sub> *Sci. Rep.* **4** 3987
- [38] Mishra R, Zhou W, Pennycook S J, Pantelides S T and Idrobo J C 2013 Long-range ferromagnetic ordering in manganese-doped two-dimensional dichalcogenides *Phys. Rev. B* **88** 144409
- [39] Lu S C and Leburton J P 2014 Electronic structures of defects and magnetic impurities in MoS<sub>2</sub> monolayers *Nanoscale Res. Lett.* **9** 2413
- [40] Ramasubramaniam A and Naveh D 2013 Mn-doped monolayer MoS<sub>2</sub>: an atomically thin dilute magnetic semiconductor *Phys. Rev. B* **87** 195201
- [41] Zhang K et al 2015 Manganese doping of monolayer MoS<sub>2</sub>: the substrate is critical *Nano Lett.* **15** 6586
- [42] Laskar M R, Nath D N, Ma L, Lee E W II, Lee C H, Kent T, Yang Z, Mishra R, Roldan M A and Idrobo J-C 2014 P-type doping of MoS<sub>2</sub> thin films using Nb *Appl. Phys. Lett.* **104** 092104
- [43] Suh J et al 2014 Doping against the native propensity of MoS<sub>2</sub>: degenerate hole doping by cation substitution *Nano Lett.* **14** 6976
- [44] Wang S Y, Ko T S, Huang C C, Lin D Y and Huang Y S 2014 Optical and electrical properties of MoS<sub>2</sub> and Fe-doped MoS<sub>2</sub> *Japan. J. Appl. Phys.* **53** 04EH07
- [45] Lin Y C, Dumcenco D O, Komasa H P, Niimi Y, Krasheninnikov A V, Huang Y S and Suenaga K 2014 Properties of individual dopant atoms in single-layer MoS<sub>2</sub>: atomic structure, migration, and enhanced reactivity *Adv. Mater.* **26** 2857

- [46] Li B, Huang L, Zhong M, Huo N, Li Y, Yang S, Fan C, Yang J, Hu W and Wei Z 2015 Synthesis and transport properties of large-scale alloy  $\text{Co}_{0.16}\text{Mo}_{0.84}\text{S}_2$  bilayer nanosheets *ACS Nano* **9** 1257
- [47] Komsa H P, Kotakoski J, Kurasch S, Lehtinen O, Kaiser U and Krasheninnikov A V 2012 Two-dimensional transition metal dichalcogenides under electron irradiation: defect production and doping *Phys. Rev. Lett.* **109** 035503
- [48] Sun L, Hu H, Zhan D, Yan J, Liu L, Teguh J S, Yeow E K, Lee P S and Shen Z 2014 Plasma modified  $\text{MoS}_2$  nanoflakes for surface enhanced Raman scattering *Small* **10** 1090
- [49] Kang N R, Paudel H P, Leuenberger M N, Tetard L and Khondaker S I 2014 Photoluminescence quenching in single-layer  $\text{MoS}_2$  via oxygen plasma treatment *J. Phys. Chem. C* **118** 21258
- [50] Islam M R, Kang N, Bhanu U, Paudel H P, Erementchouk M, Tetard L, Leuenberger M N and Khondaker S I 2014 Tuning the electrical property via defect engineering of single layer  $\text{MoS}_2$  by oxygen plasma *Nanoscale* **6** 10033
- [51] Nan H Y et al 2014 Strong photoluminescence enhancement of  $\text{MoS}_2$  through defect engineering and oxygen bonding *ACS Nano* **8** 5738
- [52] Krivanek O L et al 2010 Atom-by-atom structural and chemical analysis by annular dark-field electron microscopy *Nature* **464** 571
- [53] Ataca C and Ciraci S 2011 Functionalization of single-layer  $\text{MoS}_2$  honeycomb structures *J. Phys. Chem. C* **115** 13303
- [54] Park K T, Hess J S and Klier K 1999 Electron transfer reactions on  $\text{Cs/MoS}_2(0002)$  with chlorine, oxygen, and water: high resolution x-ray photoelectron spectroscopy and theoretical study *J. Chem. Phys.* **111** 1636
- [55] He J G, Wu K C, Sa R J, Li Q H and Wei Y Q 2010 Magnetic properties of nonmetal atoms absorbed  $\text{MoS}_2$  monolayers *Appl. Phys. Lett.* **96** 082504
- [56] Mouri S, Miyauchi Y and Matsuda K 2013 Tunable photoluminescence of monolayer  $\text{MoS}_2$  via chemical doping *Nano Lett.* **13** 5944
- [57] Komsa H-P, Kurasch S, Lehtinen O, Kaiser U and Krasheninnikov A V 2013 From point to extended defects in two-dimensional  $\text{MoS}_2$ : evolution of atomic structure under electron irradiation *Phys. Rev. B* **88** 035301
- [58] Han Y, Hu T, Li R, Zhou J and Dong J M 2015 Stabilities and electronic properties of monolayer  $\text{MoS}_2$  with one or two sulfur line vacancy defects *Phys. Chem. Chem. Phys.* **17** 3813
- [59] Zou X, Liu Y and Yakobson B I 2013 Predicting dislocations and grain boundaries in two-dimensional metal-disulfides from the first principles *Nano Lett.* **13** 253
- [60] Lehtinen O et al 2015 Atomic scale microstructure and properties of Se-deficient two-dimensional  $\text{MoSe}_2$  *ACS Nano* **9** 3274
- [61] Lin J, Pantelides S T and Zhou W 2015 Vacancy-induced formation and growth of inversion domains in transition-metal dichalcogenide monolayer *ACS Nano* **9** 5189
- [62] Azizi A, Zou X, Ercius P, Zhang Z, Elias A L, Perea-Lopez N, Stone G, Terrones M, Yakobson B I and Alem N 2014 Dislocation motion and grain boundary migration in two-dimensional tungsten disulphide *Nat. Commun.* **5** 4867
- [63] Schweiger H, Raybaud P, Kresse G and Toulhoat H 2002 Shape and edge sites modifications of  $\text{MoS}_2$  catalytic nanoparticles induced by working conditions: a theoretical study *J. Catal.* **207** 76
- [64] Meyer J C, Geim A K, Katsnelson M I, Novoselov K S, Booth T J and Roth S 2007 The structure of suspended graphene sheets *Nature* **446** 60
- [65] Luo S W, Hao G L, Fan Y P, Kou L Z, He C Y, Qi X, Tang C, Li J, Huang K and Zhong J X 2015 Formation of ripples in atomically thin  $\text{MoS}_2$  and local strain engineering of electrostatic properties *Nanotechnology* **26** 105705
- [66] Brivio J, Alexander D T and Kis A 2011 Ripples and layers in ultrathin  $\text{MoS}_2$  membranes *Nano Lett.* **11** 5148
- [67] Liu H and Chi D 2015 Dispersive growth and laser-induced rippling of large-area singleglayer  $\text{MoS}_2$  nanosheets by CVD on c-plane sapphire substrate *Sci. Rep.* **5** 11756
- [68] Miró P, Ghorbani-Asl M and Heine T 2013 Spontaneous ripple formation in  $\text{MoS}_2$  monolayers: electronic structure and transport effects *Adv. Mater.* **25** 5473
- [69] Hsu W T, Zhao Z A, Li L J, Chen C H, Chiu M H, Chang P S, Chou Y C and Chang W H 2014 Second harmonic generation from artificially stacked transition metal dichalcogenide twisted bilayers *ACS Nano* **8** 2951
- [70] Crowne F J, Amani M, Birdwell A G, Chin M L, O'Regan T P, Najmaei S, Liu Z, Ajayan P M, Lou J and Dubey M 2013 Blueshift of the A-exciton peak in folded monolayer 1H- $\text{MoS}_2$  *Phys. Rev. B* **88** 235302
- [71] Geim A K and Grigorieva I V 2013 Van der Waals heterostructures *Nature* **499** 419
- [72] Lin Y C et al 2014 Direct synthesis of van der Waals solids *ACS Nano* **8** 3715
- [73] Kang J, Li J, Li S S, Xia J B and Wang L W 2013 Electronic structural Moire pattern effects on  $\text{MoS}_2/\text{MoSe}_2$  2D heterostructures *Nano Lett.* **13** 5485
- [74] Azizi A et al 2015 Freestanding van der waals heterostructures of graphene and transition metal dichalcogenides *ACS Nano* **9** 4882
- [75] Terrones H and Terrones M 2014 Electronic and vibrational properties of defective transition metal dichalcogenide Haeckelites: new 2D semi-metallic systems *2D Mater.* **1** 011003
- [76] Terrones H, Terrones M, Hernandez E, Grobert N, Charlier J C and Ajayan P M 2000 New metallic allotropes of planar and tubular carbon *Phys. Rev. Lett.* **84** 1716
- [77] Crespi V H, Benedict L X, Cohen M L and Louie S G 1996 Prediction of a pure-carbon planar covalent metal *Phys. Rev. B* **53** R13303
- [78] Terrones H et al 2014 New first order Raman-active modes in few layered transition metal dichalcogenides *Sci. Rep.* **4** 4215
- [79] Enyashin A N, Bar-Sadan M, Houben L and Seifert G 2013 Line defects in molybdenum disulfide layers *J. Phys. Chem. C* **117** 10842
- [80] Li H, Lu G, Wang Y, Yin Z, Cong C, He Q, Wang L, Ding F, Yu T and Zhang H 2013 Mechanical exfoliation and characterization of single- and few-layer nanosheets of  $\text{WSe}_2$ ,  $\text{TaS}_2$ , and  $\text{TaSe}_2$  *Small* **9** 1974
- [81] Zeng Q, Wang H, Fu W, Gong Y, Zhou W, Ajayan P M, Lou J and Liu Z 2015 Band engineering for novel two-dimensional atomic layers *Small* **11** 1868
- [82] Dumcenco D O, Kobayashi H, Liu Z, Huang Y S and Suenaga K 2013 Visualization and quantification of transition metal atomic mixing in  $\text{Mo}_{1-x}\text{W}_x\text{S}_2$  single layers *Nat. Commun.* **4** 1351
- [83] Feng Q, Zhu Y, Hong J, Zhang M, Duan W, Mao N, Wu J, Xu H, Dong F and Lin F 2014 Growth of large-area 2D  $\text{MoS}_{2(1-x)}\text{Se}_{2x}$  semiconductor alloys *Adv. Mater.* **26** 2648
- [84] Li H, Zhang Q, Duan X, Wu X, Fan X, Zhu X, Zhuang X, Hu W, Zhou H and Pan A 2015 Lateral growth of composition graded atomic layer  $\text{MoS}_{(1-x)}\text{Se}_{2x}$  nanosheets *J. Am. Chem. Soc.* **137** 5284
- [85] Zhang M et al 2014 Two-dimensional molybdenum tungsten diselenide alloys: photoluminescence, Raman scattering, and electrical transport *ACS Nano* **8** 7130
- [86] Tongay S, Narang D S, Kang J, Fan W, Ko C, Luce A V, Wang K X, Suh J, Patel K and Pathak V 2014 Two-dimensional semiconductor alloys: monolayer  $\text{Mo}_{1-x}\text{W}_x\text{Se}_2$  *Appl. Phys. Lett.* **104** 012101
- [87] Shi Y, Li H and Li L J 2015 Recent advances in controlled synthesis of two-dimensional transition metal dichalcogenides via vapour deposition techniques *Chem. Soc. Rev.* **44** 2744
- [88] Gutierrez H R, Perea-Lopez N, Elias A L, Berkdemir A, Wang B, Lv R, Lopez-Urias F, Crespi V H, Terrones H and Terrones M 2013 Extraordinary room-temperature photoluminescence in triangular  $\text{WS}_2$  monolayers *Nano Lett.* **13** 3447
- [89] Peimyoo N, Shang J, Cong C, Shen X, Wu X, Yeow E K and Yu T 2013 Nonblinking, intense two-dimensional light emitter: monolayer  $\text{WS}_2$  triangles *ACS Nano* **7** 10985

- [90] van der Zande A M, Huang P Y, Chenet D A, Berkelbach T C, You Y, Lee G H, Heinz T F, Reichman D R, Muller D A and Hone J C 2013 Grains and grain boundaries in highly crystalline monolayer molybdenum disulphide *Nat. Mater.* **12** 554
- [91] Chow P K *et al* 2015 Wetting of mono and few-layered WS<sub>2</sub> and MoS<sub>2</sub> films supported on Si/SiO<sub>2</sub> substrates *ACS Nano* **9** 3023
- [92] Elias A L *et al* 2013 Controlled synthesis and transfer of large-area WS<sub>2</sub> sheets: from single layer to few layers *ACS Nano* **7** 5235
- [93] Su S-H, Hsu W-T, Hsu C-L, Chen C-H, Chiu M-H, Lin Y-C, Chang W-H, Suenaga K, He J-H and Li L-J 2014 Controllable synthesis of band-gap-tunable and monolayer transition-metal dichalcogenide alloys *Frontiers Energy Res.* **2** 27
- [94] Ma Q *et al* 2014 Postgrowth tuning of the bandgap of single-layer molybdenum disulfide films by sulfur/selenium exchange *ACS Nano* **8** 4672
- [95] Ji Q, Zhang Y, Zhang Y and Liu Z 2015 Chemical vapour deposition of group-VIB metal dichalcogenide monolayers: engineered substrates from amorphous to single crystalline *Chem. Soc. Rev.* **44** 2587
- [96] Cançado L G, Jorio A, Ferreira E M, Stavale F, Achete C, Capaz R, Moutinho M, Lombardo A, Kulmala T and Ferrari A 2011 Quantifying defects in graphene via Raman spectroscopy at different excitation energies *Nano Lett.* **11** 3190
- [97] Zan R, Ramasse Q M, Jalil R, Georgiou T, Bangert U and Novoselov K S 2013 Control of radiation damage in MoS<sub>2</sub> by graphene encapsulation *ACS Nano* **7** 10167
- [98] Chow P K, Jacobs-Gedrim R B, Gao J, Lu T M, Yu B, Terrones H and Koratkar N 2015 Defect-induced photoluminescence in monolayer semiconducting transition metal dichalcogenides *ACS Nano* **9** 1520
- [99] Liu Y, Nan H, Wu X, Pan W, Wang W, Bai J, Zhao W, Sun L, Wang X and Ni Z 2013 Layer-by-layer thinning of MoS<sub>2</sub> by plasma *ACS Nano* **7** 4202
- [100] Chen M K, Nam H, Wi S, Priessnitz G, Gunawan I M and Liang X G 2014 Multibit data storage states formed in plasma-treated MoS<sub>2</sub> transistors *ACS Nano* **8** 4023
- [101] Wei X X, Yu Z H, Hu F R, Cheng Y, Yu L W, Wang X Y, Xiao M, Wang J Z, Wang X R and Shi Y 2014 Mo–O bond doping and related-defect assisted enhancement of photoluminescence in monolayer MoS<sub>2</sub> *AIP Adv.* **4** 123004
- [102] Kim T Y, Cho K, Park W, Park J, Song Y, Hong S, Hong W K and Lee T 2014 Irradiation effects of high-energy proton beams on MoS<sub>2</sub> field effect transistors *ACS Nano* **8** 2774
- [103] Yamamoto M, Dutta S, Aikawa S, Nakaharai S, Wakabayashi K, Fuhrer M S, Ueno K and Tsukagoshi K 2015 Self-limiting layer-by-layer oxidation of atomically thin WSe<sub>2</sub> *Nano Lett.* **15** 2067
- [104] Castellanos-Gomez A, Barkelid M, Goossens A M, Calado V E, van der Zant H S J and Steele G A 2012 Laser-Thinning of MoS<sub>2</sub>: on demand generation of a single-layer semiconductor *Nano Lett.* **12** 3187
- [105] McDonnell S, Addou R, Buie C, Wallace R M and Hinkle C L 2014 Defect-dominated doping and contact resistance in MoS<sub>2</sub> *ACS Nano* **8** 2880
- [106] Qiu H *et al* 2013 Hopping transport through defect-induced localized states in molybdenum disulphide *Nat. Commun.* **4** 2642
- [107] Huang Y L, Chen Y, Zhang W, Quck S Y, Chen C-H, Li L-J, Hsu W-T, Chang W-H, Zheng Y J and Chen W 2015 Bandgap tunability at single-layer molybdenum disulphide grain boundaries *Nat. Commun.* **6** 6298
- [108] Ghorbani-Asl M, Enyashin A N, Kuc A, Seifert G and Heine T 2013 Defect-induced conductivity anisotropy in MoS<sub>2</sub> monolayers *Phys. Rev. B* **88** 245440
- [109] Kang K, Xie S, Huang L, Han Y, Huang P Y, Mak K F, Kim C J, Muller D and Park J 2015 High-mobility three-atom-thick semiconducting films with wafer-scale homogeneity *Nature* **520** 656
- [110] Sangwan V K, Jariwala D, Kim I S, Chen K S, Marks T J, Lauhon L J and Hersam M C 2015 Gate-tunable memristive phenomena mediated by grain boundaries in single-layer MoS<sub>2</sub> *Nat. Nanotechnol.* **10** 403
- [111] Terrones H, Lopez-Urias F and Terrones M 2013 Novel hetero-layered materials with tunable direct band gaps by sandwiching different metal disulfides and diselenides *Sci. Rep.* **3** 1549
- [112] Kompa H P and Krasheninnikov A V 2013 Electronic structures and optical properties of realistic transition metal dichalcogenide heterostructures from first principles *Phys. Rev. B* **88** 085318
- [113] Rivera P *et al* 2015 Observation of long-lived interlayer excitons in monolayer MoSe<sub>2</sub>–WSe<sub>2</sub> heterostructures *Nat. Commun.* **6** 6242
- [114] Fang H *et al* 2014 Strong interlayer coupling in van der Waals heterostructures built from single-layer chalcogenides *Proc. Natl Acad. Sci. USA* **111** 6198
- [115] Tongay S *et al* 2014 Tuning interlayer coupling in large-area heterostructures with CVD-grown MoS<sub>2</sub> and WS<sub>2</sub> monolayers *Nano Lett.* **14** 3185
- [116] Yuan J, Najmaei S, Zhang Z, Zhang J, Lei S, Ajayan P M, Yakobson B I and Lou J 2015 Photoluminescence quenching and charge transfer in artificial heterostacks of monolayer transition metal dichalcogenides and few-layer black phosphorus *ACS Nano* **9** 555
- [117] Yu Y *et al* 2015 Equally efficient interlayer exciton relaxation and improved absorption in epitaxial and nonepitaxial MoS<sub>2</sub>/WS<sub>2</sub> heterostructures *Nano Lett.* **15** 486
- [118] Heo H *et al* 2015 Interlayer orientation-dependent light absorption and emission in monolayer semiconductor stacks *Nat. Commun.* **6** 7372
- [119] Liu K, Zhang L, Cao T, Jin C, Qiu D, Zhou Q, Zettl A, Yang P, Louie S G and Wang F 2014 Evolution of interlayer coupling in twisted molybdenum disulfide bilayers *Nat. Commun.* **5** 4966
- [120] Chiu M H, Li M Y, Zhang W, Hsu W T, Chang W H, Terrones M, Terrones H and Li L J 2014 Spectroscopic signatures for interlayer coupling in MoS<sub>2</sub>–WSe<sub>2</sub> van der Waals stacking *ACS Nano* **8** 9649
- [121] Zhang K *et al* 2015 Self-induced uniaxial strain in MoS<sub>2</sub> monolayers with local van der Waals-stacked interlayer interactions *ACS Nano* **9** 2704
- [122] Lee C H *et al* 2014 Atomically thin p–n junctions with van der Waals heterointerfaces *Nat. Nanotechnol.* **9** 676
- [123] Cheng R, Li D, Zhou H, Wang C, Yin A, Jiang S, Liu Y, Chen Y, Huang Y and Duan X 2014 Electroluminescence and photocurrent generation from atomically sharp WSe<sub>2</sub>/MoS<sub>2</sub> heterojunction p–n diodes *Nano Lett.* **14** 5590
- [124] Lin Y C *et al* 2015 Atomically thin resonant tunnel diodes built from synthetic van der Waals heterostructures *Nat. Commun.* **6** 7311
- [125] McCreary A *et al* 2016 Distinct photoluminescence and Raman spectroscopy signatures for identifying highly crystalline WS<sub>2</sub> monolayers produced by different growth methods *J. Mater. Res.* accepted
- [126] Lucking M C, Bang J, Terrones H, Sun Y Y and Zhang S 2015 Multivalency-induced band gap opening at MoS<sub>2</sub> edges *Chem. Mater.* **27** 3326
- [127] Kang J, Tongay S, Zhou J, Li J B and Wu J Q 2013 Band offsets and heterostructures of two-dimensional semiconductors *Appl. Phys. Lett.* **102** 012111
- [128] Malard L M, Alencar T V, Barboza A P M, Mak K F and de Paula A M 2013 Observation of intense second harmonic generation from MoS<sub>2</sub> atomic crystals *Phys. Rev. B* **87** 201401
- [129] Kumar N, Najmaei S, Cui Q, Ceballos F, Ajayan P M, Lou J and Zhao H 2013 Second harmonic microscopy of monolayer MoS<sub>2</sub> *Phys. Rev. B* **87** 161403
- [130] Li Y, Rao Y, Mak K F, You Y, Wang S, Dean C R and Heinz T F 2013 Probing symmetry properties of few-layer MoS<sub>2</sub> and h-BN by optical second-harmonic generation *Nano Lett.* **13** 3329

- [131] Yin X B, Ye Z L, Chenet D A, Ye Y, O'Brien K, Hone J C and Zhang X 2014 Edge nonlinear optics on a MoS<sub>2</sub> atomic monolayer *Science* **344** 488
- [132] Katzke H, Toledano P and Depmeier W 2004 Phase transitions between polytypes and intralayer superstructures in transition metal dichalcogenides *Phys. Rev. B* **69** 134111
- [133] Luo X, Zhao Y, Zhang J, Toh M, Kloc C, Xiong Q and Quek S Y 2013 Effects of lower symmetry and dimensionality on Raman spectra in two-dimensional WSe<sub>2</sub> *Phys. Rev. B* **88** 195313
- [134] Yamamoto M, Wang S T, Ni M Y, Lin Y F, Li S L, Aikawa S, Jian W B, Ueno K, Wakabayashi K and Tsukagoshi K 2014 Strong enhancement of Raman scattering from a bulk-inactive vibrational mode in few-layer MoTe<sub>2</sub> *ACS Nano* **8** 3895
- [135] Carvalho B R, Malard L M, Alves J M, Fantini C and Pimenta M A 2015 Symmetry-dependent exciton-phonon coupling in 2D and Bulk MoS<sub>2</sub> observed by resonance Raman scattering *Phys. Rev. Lett.* **114** 136403
- [136] Pimenta M A, Del Corro E, Carvalho B R, Fantini C and Malard L M 2015 Comparative study of Raman spectroscopy in graphene and MoS<sub>2</sub>-type transition metal dichalcogenides *Acc. Chem. Res.* **48** 41
- [137] Carvalho B R, Hao Y, Righi A, Rodriguez-Nieva J F, Colombo L, Ruoff R S, Pimenta M A and Fantini C 2015 Probing carbon isotope effects on the Raman spectra of graphene with different <sup>13</sup>C concentrations *Phys. Rev. B* **92** 125406
- [138] Lee C, Yan H, Brus L E, Heinz T F, Hone J and Ryu S 2010 Anomalous lattice vibrations of single- and few-layer MoS<sub>2</sub> *ACS Nano* **4** 2695
- [139] Berkdemir A et al 2013 Identification of individual and few layers of WS<sub>2</sub> using Raman spectroscopy *Sci. Rep.* **3** 1755
- [140] Chakraborty B, Bera A, Muthu D, Bhowmick S, Waghmare U V and Sood A 2012 Symmetry-dependent phonon renormalization in monolayer MoS<sub>2</sub> transistor *Phys. Rev. B* **85** 161403
- [141] Conley H J, Wang B, Ziegler J I, Haglund R F Jr, Pantelides S T and Bolotin K I 2013 Bandgap engineering of strained monolayer and bilayer MoS<sub>2</sub> *Nano Lett.* **13** 3626
- [142] Bissett M A, Tsuji M and Ago H 2014 Strain engineering of the properties of graphene and other two-dimensional crystals *Phys. Chem. Chem. Phys.* **16** 11124
- [143] Pimenta M A, Dresselhaus G, Dresselhaus M S, Cancado L G, Jorio A and Saito R 2007 Studying disorder in graphite-based systems by Raman spectroscopy *Phys. Chem. Chem. Phys.* **9** 1276
- [144] Malard L M, Pimenta M A, Dresselhaus G and Dresselhaus M S 2009 Raman spectroscopy in graphene *Phys. Rep.* **473** 51
- [145] Tan P H et al 2012 The shear mode of multilayer graphene *Nat. Mater.* **11** 294
- [146] Plechinger G, Heydrich S, Eroms J, Weiss D, Schüller C and Korn T 2012 Raman spectroscopy of the interlayer shear mode in few-layer MoS<sub>2</sub> flakes *Appl. Phys. Lett.* **101** 101906
- [147] Zeng H, Zhu B, Liu K, Fan J, Cui X and Zhang Q M 2012 Low-frequency Raman modes and electronic excitations in atomically thin MoS<sub>2</sub> films *Phys. Rev. B* **86** 241301
- [148] Zhang X, Han W P, Wu J B, Milana S, Lu Y, Li Q Q, Ferrari A C and Tan P H 2013 Raman spectroscopy of shear and layer breathing modes in multilayer MoS<sub>2</sub> *Phys. Rev. B* **87** 115413
- [149] Zhao Y et al 2013 Interlayer breathing and shear modes in few-trilayer MoS<sub>2</sub> and WSe<sub>2</sub> *Nano Lett.* **13** 1007
- [150] Lee J U, Park J, Son Y W and Cheong H 2015 Anomalous excitonic resonance Raman effects in few-layered MoS<sub>2</sub> *Nanoscale* **7** 3229
- [151] Lui C H et al 2015 Observation of interlayer phonon modes in van der Waals heterostructures *Phys. Rev. B* **91** 165403
- [152] Puretzky A A et al 2015 Low-frequency Raman fingerprints of two-dimensional metal dichalcogenide layer stacking configurations *ACS Nano* **9** 6333
- [153] Mathew S et al 2012 Magnetism in MoS<sub>2</sub> induced by proton irradiation *Appl. Phys. Lett.* **101** 102103
- [154] Tongay S, Varnoosfaderani S S, Appleton B R, Wu J Q and Hebard A F 2012 Magnetic properties of MoS<sub>2</sub>: existence of ferromagnetism *Appl. Phys. Lett.* **101** 123105
- [155] Zhang J, Soon J M, Loh K P, Yin J, Ding J, Sullivan M B and Wu P 2007 Magnetic molybdenum disulfide nanosheet films *Nano Lett.* **7** 2370
- [156] Yang Z, Gao D, Zhang J, Xu Q, Shi S, Tao K and Xue D 2015 Realization of high Curie temperature ferromagnetism in atomically thin MoS<sub>2</sub> and WS<sub>2</sub> nanosheets with uniform and flower-like morphology *Nanoscale* **7** 650
- [157] Huo N J, Li Y, Kang J, Li R X, Xia Q L and Li J B 2014 Edge-states ferromagnetism of WS<sub>2</sub> nanosheets *Appl. Phys. Lett.* **104** 202406
- [158] Zhang Z, Zou X, Crespi V H and Yakobson B I 2013 Intrinsic magnetism of grain boundaries in two-dimensional metal dichalcogenides *ACS Nano* **7** 10475
- [159] Shu H, Luo P, Liang P, Cao D and Chen X 2015 Layer-dependent dopant stability and magnetic exchange coupling of iron-doped MoS<sub>2</sub> nanosheets *ACS Appl. Mater. Interfaces* **7** 7534
- [160] Yun W S and Lee J 2014 Unexpected strong magnetism of Cu doped single-layer MoS<sub>2</sub> and its origin *Phys. Chem. Chem. Phys.* **16** 8990
- [161] Lin X and Ni J 2014 Charge and magnetic states of Mn-, Fe-, and Co-doped monolayer MoS<sub>2</sub> *J. Appl. Phys.* **116** 044311
- [162] Yue Q, Chang S, Qin S and Li J 2013 Functionalization of monolayer MoS<sub>2</sub> by substitutional doping: a first-principles study *Phys. Lett. A* **377** 1362
- [163] Hinemann B, Moses P G, Bonde J, Jørgensen K P, Nielsen J H, Horch S, Chorkendorff I and Nørskov J K 2005 Biomimetic hydrogen evolution: MoS<sub>2</sub> nanoparticles as catalyst for hydrogen evolution *J. Am. Chem. Soc.* **127** 5308
- [164] Rao C, Maitra U and Waghmare U V 2014 Extraordinary attributes of 2-dimensional MoS<sub>2</sub> nanosheets *Chem. Phys. Lett.* **609** 172
- [165] Jaramillo T F, Jørgensen K P, Bonde J, Nielsen J H, Horch S and Chorkendorff I 2007 Identification of active edge sites for electrochemical H<sub>2</sub> evolution from MoS<sub>2</sub> nanocatalysts *Science* **317** 100
- [166] Kong D, Wang H, Cha J J, Pasta M, Koski K J, Yao J and Cui Y 2013 Synthesis of MoS<sub>2</sub> and MoSe<sub>2</sub> films with vertically aligned layers *Nano Lett.* **13** 1341
- [167] Wang H, Kong D, Johanes P, Cha J J, Zheng G, Yan K, Liu N and Cui Y 2013 MoSe<sub>2</sub> and WSe<sub>2</sub> nanofilms with vertically aligned molecular layers on curved and rough surfaces *Nano Lett.* **13** 3426
- [168] Wu Z Z, Fang B Z, Wang Z P, Wang C L, Liu Z H, Liu F Y, Wang W, Alfantazi A, Wang D Z and Wilkinson D P 2013 MoS<sub>2</sub> nanosheets: a designed structure with high active site density for the hydrogen evolution reaction *ACS Catal.* **3** 2101
- [169] Xie J, Zhang J, Li S, Grote F, Zhang X, Zhang H, Wang R, Lei Y, Pan B and Xie Y 2013 Controllable disorder engineering in oxygen-incorporated MoS<sub>2</sub> ultrathin nanosheets for efficient hydrogen evolution *J. Am. Chem. Soc.* **135** 17881
- [170] Xie J, Zhang H, Li S, Wang R, Sun X, Zhou M, Zhou J, Lou X W and Xie Y 2013 Defect-rich MoS<sub>2</sub> ultrathin nanosheets with additional active edge sites for enhanced electrocatalytic hydrogen evolution *Adv. Mater.* **25** 5807
- [171] Wang H et al 2013 Electrochemical tuning of vertically aligned MoS<sub>2</sub> nanofilms and its application in improving hydrogen evolution reaction *Proc. Natl Acad. Sci. USA* **110** 19701
- [172] Lukowski M A, Daniel A S, Meng F, Forticaux A, Li L and Jin S 2013 Enhanced hydrogen evolution catalysis from chemically exfoliated metallic MoS<sub>2</sub> nanosheets *J. Am. Chem. Soc.* **135** 10274
- [173] Voiry D, Salehi M, Silva R, Fujita T, Chen M W, Asefa T, Shenoy V B, Eda G and Chhowalla M 2013 Conducting MoS<sub>2</sub>

- nanosheets as catalysts for hydrogen evolution reaction *Nano Lett.* **13** 6222
- [174] Li Y, Wang H, Xie L, Liang Y, Hong G and Dai H 2011 MoS<sub>2</sub> nanoparticles grown on graphene: an advanced catalyst for the hydrogen evolution reaction *J. Am. Chem. Soc.* **133** 7296
- [175] Seifert G, Terrones H, Terrones M, Jungnickel G and Frauenheim T 2000 Structure and electronic properties of MoS<sub>2</sub> nanotubes *Phys. Rev. Lett.* **85** 146
- [176] Podila R, Rao R, Tsuchikawa R, Ishigami M and Rao A M 2012 Raman spectroscopy of folded and scrolled graphene *ACS Nano* **6** 5784
- [177] Miró P, Ghorbani-Asl M and Heine T 2013 Transition metal monolayers: spontaneous ripple formation in MoS<sub>2</sub> monolayers: electronic structure and transport effects *Adv. Mater.* **25** 5366
- [178] Chou S S, De M, Kim J, Byun S, Dykstra C, Yu J, Huang J and Dravid V P 2013 Ligand conjugation of chemically exfoliated MoS<sub>2</sub> *J. Am. Chem. Soc.* **135** 4584